

Complex Langevin Dynamics in Large N Unitary Matrix Models

Pallab Basu^a Kasi Jaswin^a and Anosh Joseph^a

^a*International Centre for Theoretical Sciences,
Tata Institute of Fundamental Research,
Bangalore, 560089 INDIA*

E-mail: pallab.basu@icts.res.in, jaswin@icts.res.in,
anosh.joseph@icts.res.in

ABSTRACT: Using complex Langevin dynamics we examine the phase structure of complex unitary matrix models and compare the numerical results with analytic results found at large N . The actions we consider are manifestly complex, and thus the dominant contribution to the path integral comes from the space of complexified gauge field configuration. For this reason, the eigenvalues of unitary matrix lie off the unit circle and venture out in the complex plane. One example of a complex unitary matrix model, with Polyakov line as the unitary matrix, is an effective description of a QCD at finite density and temperature with N number of colors and N_f number of quark flavors defined on the manifold $S^1 \times S^3$. A distinct feature of this model, the occurrence of a series of Gross-Witten-Wadia transitions, as a function of the quark chemical potential, is reproduced using complex Langevin simulations. We simulate several other observables including Polyakov lines and quark number density, for large N and N_f and found excellent match with the analytic results.

KEYWORDS: Sign problem, Complex action, Complex Langevin method, QCD phase diagram, Large N matrix models

Contents

1	Introduction	1
2	Complex Langevin Dynamics	4
3	ab-Model	5
3.1	Ungapped Phase	6
3.2	Gapped Phase	10
3.3	Phase transition of <i>ab</i> -Model	14
4	Gauge Theory to Unitary Matrix Model	16
4.1	Observables	17
4.2	Single Level Model with Positive Chemical Potential	18
4.3	Single Level Model with Two Fugacities	23
4.4	Single Level Model with Interaction	24
5	Conclusions and Discussions	25
A	QCD on $S^1 \times S^3$ at Finite Chemical Potential	27
A.1	Fermion number $\langle f_N \rangle$	27
A.2	Polyakov Lines $\langle P \rangle$ and $\langle P^{-1} \rangle$	28
A.3	Pressure $\langle p \rangle$ and Energy $\langle E \rangle$	28
B	Reliability of Complex Langevin Dynamics	31

1 Introduction

A nonperturbative study of the phase structure of QCD at finite temperature and nonzero baryon chemical potential still remains an outstanding problem [1, 2]. This is due to the fact that the fermion determinant becomes complex and the theory has a sign problem. The standard methods to study the theory, lattice QCD algorithms based on importance sampling, fail to produce reliable simulations. There have been recent developments in tackling this problem. One method is the use of complex Langevin dynamics with stochastic quantization [3, 4]. This method is not based on importance sampling but instead on a stochastic exploration of an enlarged (complexified) field configuration space. Another recently proposed method is the Lefschetz thimble method [5–10], which is also based on complexification of the original real field variables.

The complex Langevin method was proposed in the early 1980s by Klauder [3, 11, 12] and Parisi [4]. Though it became popular in the beginning certain problems were found immediately after. First one was the problem of runaways, where the simulations would not

converge and the second one was the problem of convergence to a wrong limit. In recent years the complex Langevin method has been revived, with sometimes cases of impressive success [13–18]. It has been shown recently that complex Langevin simulations produce seemingly correct answer, even when the fermion sign problem is severe, for one-, three- and four-dimensional field theories with nonzero chemical potential [19–22]. There have also been studies of supersymmetric matrix models based on complex Langevin dynamics. See Refs. [23–25].

In this paper, we consider a large N unitary matrix model at low temperature with a finite quark chemical potential and quark mass. This model is obtained from the one-loop formulation of QCD on $S^1 \times S^3$ at finite temperature with finite quark chemical potential μ , quark mass m , and with N number of colors and N_f number of quark flavors. After integrating out the quark and gauge degrees of freedom we obtain the model of our interest – a conventional unitary matrix model with a complex action. The unitary matrix U in this model is the holonomy (Wilson loop) of the gauge field around the thermal time circle in Euclidean space. We can use the expectation value of the trace of Polyakov line in the fundamental representation as order parameter for the phase transitions. It is zero in the confined phase and non-zero in the deconfined phase. The model is interesting as it exhibits a rich thermal phase structure. When the chemical potential passes one of the quark energy levels there is a third order Gross-Witten-Wadia (GWW) transition from a confined to a deconfined phase and back again. This model also exhibits another interesting feature known as the *Silver Blaze* behavior. When the quark mass is nonvanishing the bulk observables of the model are nearly zero until the onset transition to the deconfined phase, which occurs when the chemical potential reaches the value of the lightest quark mass.

In the matrix model with complex action, the dominant contributions to the functional integral come from complexified gauge field configurations. Due to this reason, the saddle point eigenvalues of the unitary matrix U lie off the unit circle, on a contour in the complex plane. The eigenvalues of U can be written as $\exp(i\theta_i)$ with θ_i the angle variables and $i = 1, \dots, N$. We can make a change of variables such that the functional integral reduces to an integral over $\{\theta_i\}$. At large N , the functional integral is dominated by a single saddle point but since the action is complex this saddle point configuration lies out in the complex plane where the θ_i are no longer real. As a consequence, the Polyakov line and the inverse Polyakov line are not equal, that is, $\langle P \rangle \neq \langle P^{-1} \rangle$. Through complex Langevin simulations we indeed confirm this behavior. In fact the behavior of inverse Polyakov line precedes that of the Polyakov line as a function of chemical potential. This feature was observed analytically in an earlier work by Hands, Hollowood and Myers in Ref. [26].

In this paper, we examine this large N unitary matrix models using complex Langevin simulations. It is possible to generate representative field configurations by integrating a stochastic differential equation, known as the complex Langevin equation. The drift terms arising from the complex action force the field variables to evolve in an extended (complexified) field space, in which the large regions where the observables are plagued by phase fluctuations are avoided [17].

When N is large, we can consider the gauge field, corresponding to the angles of the Polyakov line, as a distribution on a contour. From the equation of motion, the saddle point

distribution of the Polyakov line eigenvalues can be calculated analytically and plotted by mapping the angles from an arc on the unit circle to a contour over the same range of angles in the complex plane [26]. The theory is said to be in a confined phase when the contour on which the Polyakov line eigenvalues are distributed is closed. The contour opens up in between quark energy level transitions giving rise to a deconfined phase in the theory. The third derivative of the grand potential is discontinuous at each energy level crossing. These are characteristic features of a third order, GWW transition [27–29].

This paper is organized as follows. In Sec. 2 we give a brief outline of complex Langevin dynamics and stochastic quantization. In Sec. 3 we discuss a simple yet nontrivial matrix model called the ab-Model, which is a complexified version of the Gross-Witten-Wadia (GWW) model. This model has two phases, confined and deconfined, and it exhibits a third-order phase transition. In Sec. 4 we discuss another interesting large N unitary matrix model which arises in the one-loop formulation of QCD on compact spaces. The model possess a tower of quark energy levels due to compactification and is defined for positive and negative chemical potential values. We then focus on to a truncated cousin of this model - a single quark energy level matrix model with positive chemical potential. This model also has a complex action and captures the physics we are interested in without loss of generality. We can define an effective fugacity in this model, and as we change the fugacity, the model exhibits confinement/deconfinement phase transitions. We show the eigenvalue distributions corresponding to the confined (closed) and deconfined (gapped) phases of the theory using complex Langevin simulations. We also simulate the behaviors of Polyakov lines and fermion number density as a function of effective fugacity. We simulate the model for a range of temperatures and chemical potentials to study its phase structure. We also show the phase diagram of the model, at low temperature, on the (μ, β) plane, in the vicinity where quark energy level equals the chemical potential. Our simulation results agree well with the schematic prediction given by Hands, Hollowood and Myers in Ref. [26]. We then simulate the model at large quark mass and show that the bulk observables exhibit the Silver Blaze behavior – the observables are roughly zero until the onset transition to the deconfined phase, which occurs when the chemical potential equals quark mass. We then move on to discuss the single-level model with a simple non-trivial gauge interaction turned on. We study the behavior of observables as a function of the interaction parameter. We see that the model prefers to stay in the confined phase as the interaction strength is increased. In Sec. 5 we provide conclusions and discussions. In Appendix. A we use complex Langevin dynamics to simulate QCD on $S^1 \times S^3$ at finite chemical potential and low temperature. We are able to reproduce the series of GWW transitions, as a function of the chemical potential, as described in Ref. [26]. Our simulations also reproduce the level structure feature of the bulk observables - fermion number density, pressure and energy - of the model. In Appendix B we investigate the probability distribution for the magnitude of the drift term.

2 Complex Langevin Dynamics

The central idea of stochastic quantization is that expectation values of observables are obtained as equilibrium values of a stochastic process [30, 31]. In order to achieve this we evolve the system in a fictitious time τ , subject to a stochastic noise. That is, the system evolves according to Langevin dynamics. When the action is complex it is still possible to consider Langevin dynamics. The force (gradient of the action) becomes complex in this case making the fields also complex during the evolution.

In this work we make use of complex Langevin dynamics with stochastic quantization to study large N unitary matrix models with complex actions. They exhibit sign problem due to the fact that the action is complex. Standard Monte Carlo methods fail to produce the correct equilibrium distributions of these models. We can use discretized complex Langevin equation with Euler method (which is a first order algorithm) to find the equilibrium field distributions of these models.

Let us take $\theta_i(\tau)$ with $i = 1, \dots, N$ as the complexified angle variables of the gauge link $U(\tau)$ at a Langevin time τ . We have the discrete Langevin evolution equation

$$\theta_i(\tau + \Delta\tau) = \theta_i(\tau) - \left[\frac{\partial S}{\partial \theta_i(\tau)} \right] \Delta\tau + \sqrt{\Delta\tau} \eta_i(\tau), \quad (2.1)$$

where $\Delta\tau$ is the Langevin time step, and $\eta_i(\tau)$ is a Gaussian random variable satisfying the conditions

$$\langle \eta_i(\tau) \rangle = 0, \quad \langle \eta_i(\tau) \eta_j(\tau') \rangle = 2\delta_{ij} \delta_{\tau\tau'}. \quad (2.2)$$

We also note that strictly at infinite N the fluctuation term in Eq. (2.1) could be safely dropped.

To reduce excursions in the imaginary directions of the field configurations, which would spoil the validity of the method, we should use real Gaussian random variables [32–34].

We also need to impose the $SU(N)$ constraint on the complexified angular variables after each Langevin time step. That is,

$$\sum_{i=1}^N \theta_i(\tau) = 0. \quad (2.3)$$

This can be easily implemented by subtracting the average value $\theta_{\text{av}}(\tau)$ from each $\theta_i(\tau)$ variable.

We note that there also exists another complementary method in which one could implement complex Langevin dynamics directly on the matrix variables $U(\tau)$. In this case the evolution equation takes the form

$$U(\tau + 1) = R(\tau)U(\tau) \quad (2.4)$$

where the matrix R is a stochastic unitary matrix. We note that this method can be used for studying similar models in higher spacetime dimensions.

In this paper, we use the first method described above where the link field U is diagonalized and the $SU(N)$ constraint is imposed.

3 ab-Model

To demonstrate the effectiveness of Complex Langevin Dynamics, we begin by studying a simple, yet non-trivial model – a complexified version of Gross-Witten-Wadia (GWW) Model [27–29, 35]. We refer to our model as *ab-Model*. It has two phases, confined and deconfined, exhibiting a third-order phase transition. The action is given by

$$S = N \left(a \text{Tr } U + b \text{Tr } U^\dagger \right) \quad (3.1)$$

where, $a, b \in \mathbb{C}$, U is an element of $SU(N)$, and $a = b$ is the Gross-Witten-Wadia model.

Before proceeding further let us make a few generic comments. A linear term in $\text{Tr } U$ breaks the center symmetry. Furthermore, the above action (or other polynomial generalization of it) is complex. If $a \neq b$, then the \mathbb{Z}_2 symmetry $U \rightarrow U^\dagger$ is broken. This implies $\langle \text{Tr } U \rangle \neq \langle \text{Tr } U^\dagger \rangle$. One may ask, that what it means in terms of manifestly gauge invariant operators. This means that the contribution from baryon and anti-baryon is different. Another related observation is one may naively expand Eq. (3.1) in series,

$$Z = \int DU e^{-S} = \int DU \left(1 + N a b \text{Tr } U \text{Tr } U^\dagger + N^2 (a b)^2 (\text{Tr } U \text{Tr } U^\dagger)^2 \dots \right) + \quad (3.2)$$

$$\left(N^N a^N \text{Tr } U^N + N^N b^N \text{Tr } U^{\dagger N} \right) + \dots$$

Here we have separated the “mesonic” and “baryonic” contributions. Due to the center symmetry only a gauge invariant combination of $\text{Tr } U$ and $\text{Tr } U^\dagger$ contributes. By mesonic contribution we mean product of traces for which sum of powers all the occurrence of unitary matrix and its inverse sum to zero. For baryonic operator, the sum is only zero up to modulo N , i.e., proportional to a non-zero integral power of N . If baryonic contributions are neglected then Eq. (3.1) is equivalent to a model with parameters, $a = b = \sqrt{ab}$. We will later see that for gauge invariant operators, this equivalence is actually held in the ungapped phase.

Expressing the action in diagonal gauge, the effective action becomes

$$S_{eff} = \sum_{i,j=1, i \neq j}^N -\frac{1}{2} \ln \left(\sin^2 \left(\frac{\theta_i - \theta_j}{2} \right) \right) + i N \mathcal{M} \sum_{i=1}^N \theta_i$$

$$+ N \left(a \sum_{i=1}^N e^{i\theta_i} + b \sum_{i=1}^N e^{-i\theta_i} \right), \quad (3.3)$$

where the first term is the Vandermonde piece, and \mathcal{M} is the Lagrange multiplier which ensures that $\det(U) = 1$.

At large N , the theory is dominated by the saddle-point equation

$$\frac{\partial S_{eff}}{\partial \theta_i} = 0, \quad (3.4)$$

which gives the equation of motion

$$i \mathcal{M} + i \left(a e^{i\theta_i} - b e^{-i\theta_i} \right) = \frac{1}{N} \sum_{j \neq i} \cot \left(\frac{\theta_i - \theta_j}{2} \right). \quad (3.5)$$

On substituting $z_i = e^{i\theta_i}$ the equation of motion becomes

$$i\mathcal{M} + ia z_i - i \left(\frac{b}{z_i} \right) = \frac{i}{N} \sum_{j \neq i} \left(\frac{z_i + z_j}{z_i - z_j} \right), \quad (3.6)$$

and \mathcal{M} is given by

$$\mathcal{M} = \frac{1}{N} \sum_{i=1}^N \left(\frac{b}{z_i} - a z_i \right). \quad (3.7)$$

In the saddle point, \mathcal{M} may have a non-zero value and could be thought as effective baryon number.

At $N \rightarrow \infty$ limit, we can replace the summation by an integral over a non-decreasing function

$$\frac{1}{N} \sum_{i=1}^N \rightarrow \int_{-\pi}^{\pi} \frac{ds}{2\pi}, \quad (3.8)$$

and performing a change of variables from s to complex variables $z(s)$

$$\frac{ids}{dz} = \rho(z), \quad (3.9)$$

the equation of motion becomes

$$\mathcal{M} + az - \left(\frac{b}{z} \right) = P \oint_C \frac{d\omega}{2\pi i} \rho(\omega) \left(\frac{z + \omega}{z - \omega} \right), \quad (3.10)$$

and P implies we are taking the principal value of the integral.

3.1 Ungapped Phase

In GWW model, it is known that for small potential, i.e., $a < 0.5$, the theory is in an ungapped phase. Assuming a similar picture also holds for the *ab-Model*, we solve it by taking an ansatz for $\rho(z)$ in ungapped phase as,

$$\rho(\omega) = A_0 + \frac{A_1}{\omega} + \frac{A_2}{\omega^2} + \dots \quad (3.11)$$

then

$$P \oint_C \frac{d\omega}{2\pi i} \rho(\omega) \left(\frac{z + \omega}{z - \omega} \right) = -A_0 z + \frac{A_2}{z} + \dots \quad (3.12)$$

Comparing with the LHS of Eq. (3.10)

$$A_0 = -a \text{ and } A_2 = -b. \quad (3.13)$$

Therefore ρ becomes,

$$\rho(z) = -a + \frac{A_1}{z} - \frac{b}{z^2} + \dots \quad (3.14)$$

We also find

$$\mathcal{M} = \oint_C \frac{dz}{2\pi i} \rho(z) \left(\frac{b}{z} - az \right) = 0, \quad (3.15)$$

which indicates that the theory is in an ungapped phase. Demanding normalization of $\rho(z)$

$$\oint \frac{dz}{2\pi i} \rho(z) = 1, \quad (3.16)$$

we fix $A_1 = 1$.

Therefore,

$$\rho(z) = \frac{1}{z} - a - \frac{b}{z^2} + \dots \quad (3.17)$$

We can solve for the contour, where $\rho(z)$ is positive definite, by integrating Eq. (3.9)

$$is = \ln(z) - az + \frac{b}{z} + c. \quad (3.18)$$

Since s is purely real, and assuming that

$$z = r(\theta)e^{i\theta}, \quad a = |a|e^{i\phi_1} \text{ and } b = |b|e^{i\phi_2}, \quad (3.19)$$

the above equation is satisfied only if the real part of the RHS is zero. That is,

$$\ln(r(\theta)) - |a|r(\theta) \cos(\theta + \phi_1) + \frac{|b|}{r(\theta)} \cos(\theta - \phi_2) + \text{Re}(c) = 0. \quad (3.20)$$

To fix c , we invoke the condition that $\det(U) = 1$, i.e., $\sum_{i=1}^N \theta_i = 0$, which translates to

$$\int_C \frac{dz}{2\pi i} \ln(z) \rho(z) = 0, \quad (3.21)$$

where the branch-cuts are taken from $z = 0$ to the point $z(\pm\pi)$. Replacing $\ln(z)$ using Eq. (3.18), the above equation becomes

$$\begin{aligned} \int \frac{dz}{2\pi i} \left(is + az - \frac{b}{z} - c \right) \rho(z) &= 0 \\ \Rightarrow -c + \oint \frac{dz}{2\pi} \rho(z) s &= 0 \\ \Rightarrow -c + i \int_{-\pi}^{\pi} \frac{ds}{2\pi} s &= 0 \\ \Rightarrow c &= 0. \end{aligned} \quad (3.22)$$

Hence the contour is got by solving the transcendental equation

$$\ln(r(\theta)) - |a|r(\theta) \cos(\theta + \phi_1) + \frac{b}{r(\theta)} \cos(\theta - \phi_2) = 0. \quad (3.23)$$

Now we can compare the distribution of eigenvalues from complex Langevin dynamics with the analytic result for any (a, b) combination. In Fig. 1 we show the analytical result and the data obtained through complex Langevin simulations without noise for parameters $a = 0.35$, $b = 0.2$ and $N = 100$. In Fig. 2 we show the result with Gaussian noise turned on. We see an excellent agreement between the analytical and numerical results.

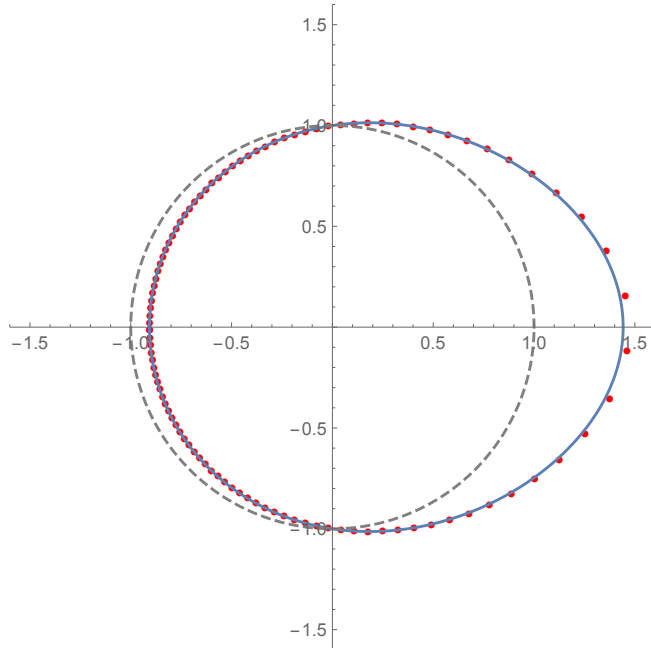


Figure 1: The distribution of eigenvalues of ab -model with parameters $a = 0.35$, $b = 0.2$ and $N = 100$. The solid curve is the analytical result and the data points are obtained through complex Langevin simulations without introducing the Gaussian noise. The dashed curve is a unit circle.

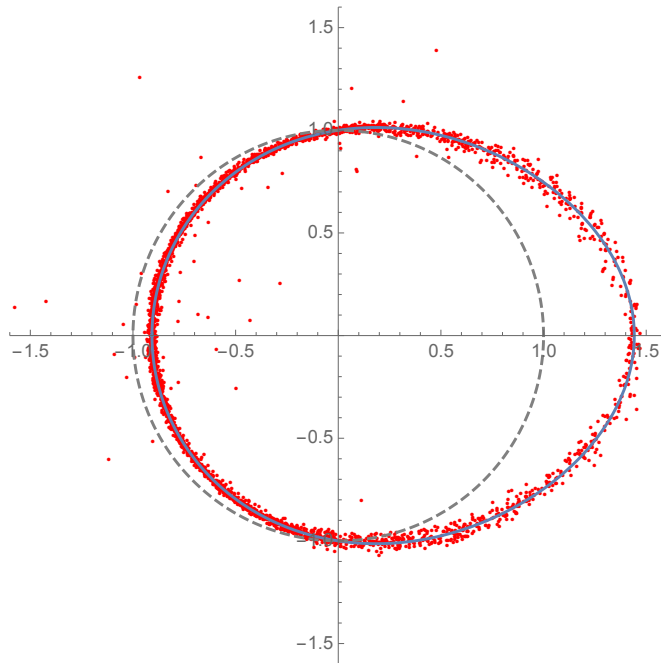


Figure 2: The distribution of eigenvalues of ab -model with parameters $a = 0.35$, $b = 0.2$ and $N = 100$. The solid curve is the analytical result and the data points are obtained through complex Langevin simulations. The dashed curve is a unit circle.

We also note that the complex Langevin simulations show excellent agreement with

analytical results when the parameters are also complex. In Fig. 3 we show the analytical result and the data obtained through complex Langevin simulations without noise for parameters $a = 0.2 + i0.2$, $b = -0.1 + i0.1$ and $N = 100$. In Fig. 4 we show the result with Gaussian noise turned on.

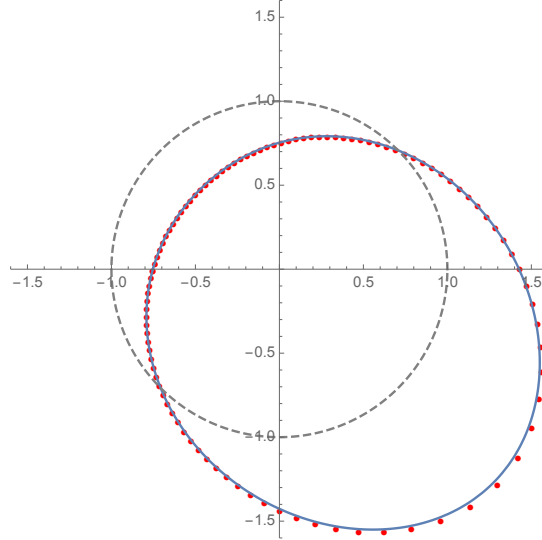


Figure 3: The distribution of eigenvalues of ab -model with parameters $a = 0.2 + i0.2$, $b = -0.1 + i0.1$ and $N = 100$. The solid curve is the analytical result and the data points are obtained through complex Langevin simulations without introducing the Gaussian noise. The dashed curve is a unit circle.

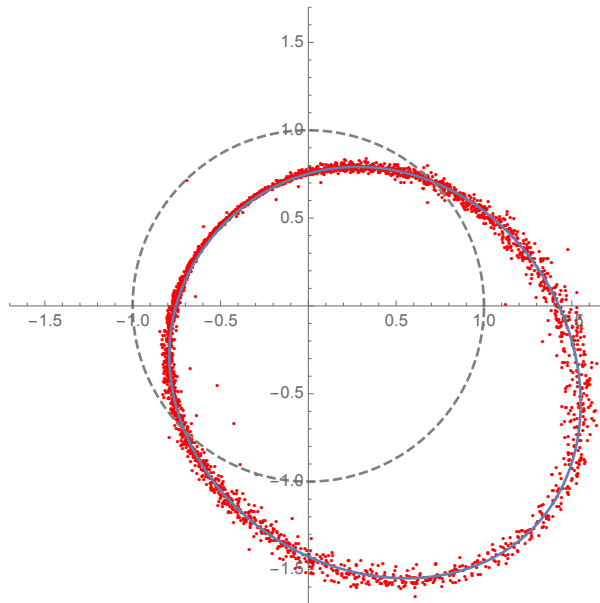


Figure 4: The distribution of eigenvalues of ab -model with parameters $a = 0.2 + i0.2$, $b = -0.1 + i0.1$ and $N = 100$. The solid curve is the analytical result and the data points are obtained through complex Langevin simulations. The dashed curve is a unit circle.

3.2 Gapped Phase

In the gapped phase, similar to GWW model, the eigenvalues lie on an open contour C .

To study this phase, we employ resolvent/spectral-curve method used in Ref. [26], and reviewed in Ref. [36]. The resolvent is defined as

$$\omega(z) = -\frac{1}{N} \sum_j \left(\frac{z + z_j}{z - z_j} \right). \quad (3.24)$$

At large N limit, $\omega(z)$ is analytic everywhere in the complex plane, except along a square-root branch cut running along C , and expressed as

$$\omega(z) = - \int_C \frac{dz'}{2\pi i} \rho(z') \frac{z + z'}{z - z'}. \quad (3.25)$$

For a given potential $V(z)$, the equation of motion (similar to Eq. (3.10))

$$zV'(z) = P \oint_C \frac{dz'}{2\pi i} \rho(z') \frac{z + z'}{z - z'} \quad (3.26)$$

can be expressed in terms of $\omega(z)$ using the Plemelj formulae

$$zV'(z) = \frac{1}{2} [\omega(z + \epsilon) + \omega(z - \epsilon)], \quad z \in C, \quad (3.27)$$

where $z \pm \epsilon$ lies on either side of the branch cut and $\epsilon \rightarrow 0$ limit is taken.

We can also express $\rho(z)$ as the discontinuity of $\omega(z)$ across the cut C as

$$z\rho(z) = \frac{1}{2} [\omega(z + \epsilon) - \omega(z - \epsilon)]. \quad (3.28)$$

The expectation value of any function $G(z)$ can be found as

$$\int_C \frac{dz}{2\pi i} \rho(z) G(z) = \oint_{\tilde{C}} \frac{dz}{4\pi i z} \omega(z) G(z). \quad (3.29)$$

For ab -model

$$\omega(z) = -\mathcal{M} - az + \frac{b}{z} + f(z) \sqrt{(z - \tilde{z})(z - \tilde{z}^*)}, \quad (3.30)$$

where \tilde{z}, \tilde{z}^* are the end points of branch cut C and $f(z)$ is an unknown function, which remains to be fixed. Since $\omega(z)$ has to be regular over the entire plane except along C and the origin we can fix the form of $f(z)$ as

$$f(z) = c + \frac{d}{z}. \quad (3.31)$$

Therefore $\omega(z)$ becomes (substituting $\tilde{z} = Re^{i\phi}$)

$$\omega(z) = -\mathcal{M} - az + \frac{b}{z} + \left(c + \frac{d}{z} \right) \sqrt{z^2 + R^2 - 2Rz \cos(\phi)}. \quad (3.32)$$

Normalization of $\rho(z)$, from Eq. (3.25), translates to

$$\lim_{|z| \rightarrow 0} \omega(z) = 1 \quad (3.33)$$

and

$$\lim_{|z| \rightarrow \infty} \omega(z) = -1. \quad (3.34)$$

This fixes $f(z)$ as

$$f(z) = a - \frac{b}{Rz}. \quad (3.35)$$

We also get two more relations between R , \mathcal{M} and $\cos(\phi)$

$$aR + \frac{b \cos(\phi)}{R} = 1 + \mathcal{M}, \quad (3.36)$$

and

$$a \cos(\phi)R + \frac{b}{R} = 1 - \mathcal{M}. \quad (3.37)$$

To fix the three unknowns completely, we need a third equation, which comes from invoking the $\det(U) = 1$ condition, from Eq. (3.29)

$$\int_{\tilde{C}} \frac{dz}{4\pi iz} \omega(z) \ln(z) = 0, \quad (3.38)$$

where \tilde{C} is a contour encircling the branch cut C , and the branch cut of $\ln(z)$ ranges from $(-\infty, 0)$. Deforming the contour Fig. 5 to the one in Fig. 6

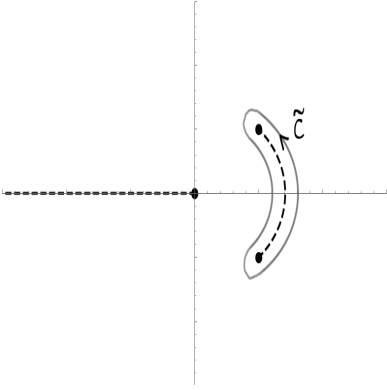


Figure 5: Actual contour over which Eq. (3.38) needs to be performed.

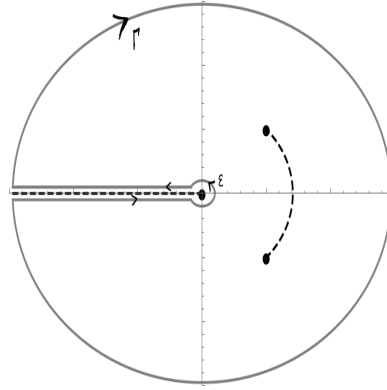


Figure 6: Deformed contour over which the integral was performed.

and evaluating in $\epsilon \rightarrow 0$ and $\Gamma \rightarrow \infty$ limits, we find that the divergences arising from the cutoffs Γ and ϵ cancel separately and we arrive at the following condition

$$\begin{aligned} \left(aR - \frac{b}{R} \right) \left[\left(\frac{1 - \cos(\phi)}{2} \right) \ln \left(\frac{1 - \cos(\phi)}{2} \right) + \left(\frac{1 + \cos(\phi)}{2} \right) \right] \\ = \left(aR + \frac{b}{R} \right) \left(\frac{1 + \cos(\phi)}{2} \right) \ln(R). \end{aligned} \quad (3.39)$$

Now for a given a, b we can numerically solve the Eqs. (3.36), (3.37), and (3.39) for R , \mathcal{M} and $\cos(\phi)$, and hence fix $\omega(z)$ completely. Also from Eq. (3.28) we can fix $\rho(z)$

$$\rho(z) = \left(\frac{a}{z} - \frac{b}{Rz^2} \right) \sqrt{z^2 + R^2 - 2Rz \cos(\phi)}. \quad (3.40)$$

From Eq. (3.15), we can numerically compute \mathcal{M} , both in ungapped and gapped phases, and compare it against analytical results. Choosing $b = 2.0a$ and varying a from 0 to 1.2, we find that it matches very well both in ungapped and gapped regimes – see Fig. 7. (Gap opening point can be found from Fig. 10.)

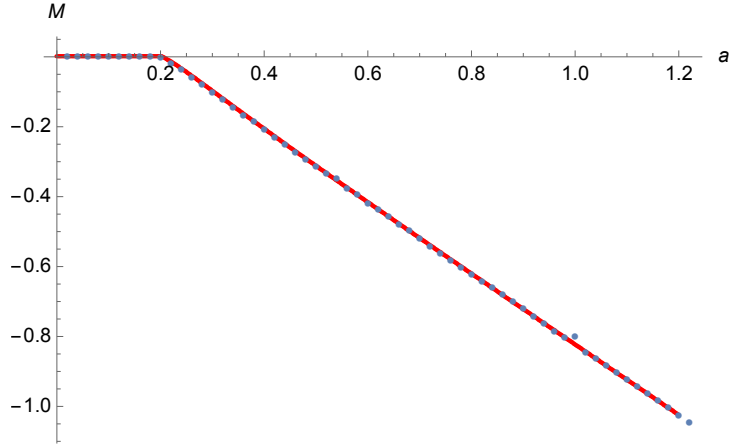


Figure 7: The value of \mathcal{M} at $(a, 2a)$ for the ab -model with $N = 100$. The solid curve is analytical result and the data points are obtained through complex Langevin simulations.

Similarly we compare other observables, $\langle \text{Tr} (U) \rangle$ and $\langle \text{Tr} (U^{-1}) \rangle$. Analytically $\langle \text{Tr} (U) \rangle$ is given by,

$$\begin{aligned} \langle \text{Tr} (U) \rangle &= \oint \frac{dz}{2\pi i} \left(\frac{1}{z} - a - \frac{b}{z^2} \right) z = -b && \text{(Ungapped)} \\ &= \oint_{\tilde{C}} \frac{dz}{4\pi i} \frac{w(z)}{z} z = \left(\frac{\cos \phi + 1}{4} \right) (a(\cos \phi - 1)R^2 - 2b) && \text{(Gapped)} \end{aligned} \quad (3.41)$$

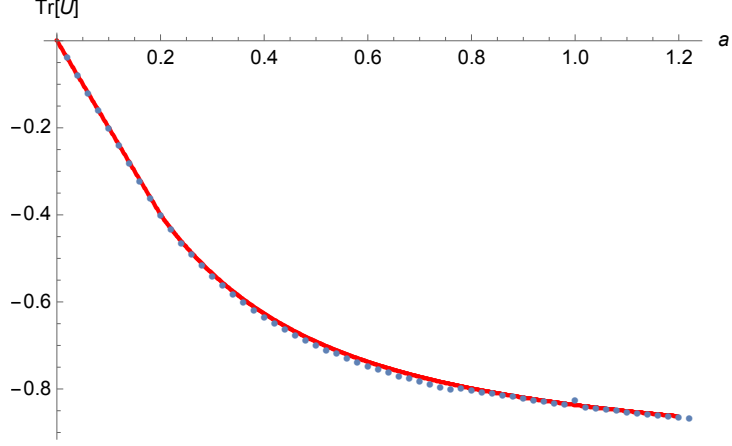


Figure 8: The value of $\text{Tr}(U)$ at $(a, 2a)$ for the ab -model with $N = 100$. The solid curve is analytical result and the data points are obtained through complex Langevin simulations.

and $\langle \text{Tr}(U^{-1}) \rangle$ by,

$$\begin{aligned}
 \langle \text{Tr}(U^{-1}) \rangle &= \oint \frac{dz}{2\pi i} \left(\frac{1}{z} - a - \frac{b}{z^2} \right) \frac{1}{z} = -a && \text{(Ungapped)} \\
 &= \oint_{\tilde{C}} \frac{dz}{4\pi i} \frac{\omega(z)}{z} \frac{1}{z} = \left(\frac{\cos \phi + 1}{4} \right) \left(\frac{b(\cos \phi - 1)}{R^2} - 2a \right) && \text{(Gapped)}
 \end{aligned} \tag{3.42}$$

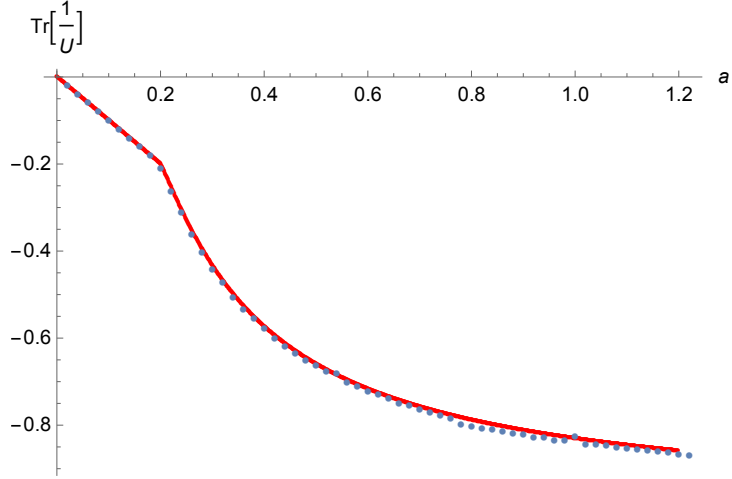


Figure 9: The value of $\text{Tr}(U^{-1})$ at $(a, 2a)$ for the ab -model with $N = 100$. The solid curve is analytical result and the data points are obtained through complex Langevin simulations.

In Fig. 8 and Fig. 9 we show the observables $\langle \text{Tr}(U) \rangle$ and $\langle \text{Tr}(U^{-1}) \rangle$, respectively. The analytical and numerical results show excellent agreement.

3.3 Phase transition of ab -Model

The eigenvalue density Eq. (3.17) on contour Eq. (3.23), is proportional to ds , which in terms of $r(\theta)$ is given by

$$\begin{aligned} ds &= \frac{d}{d\theta} \left[\theta - |a| \sin(\theta + \phi_1) r(\theta) - \frac{|b|}{r(\theta)} \sin(\theta - \phi_2) \right] d\theta \\ &= \left[1 - |a| \cos(\theta + \phi_1) r(\theta) - |a| \sin(\theta + \phi_1) r'(\theta) \right. \\ &\quad \left. - \frac{|b|}{r(\theta)} \cos(\theta - \phi_2) + \frac{|b| r'(\theta)}{r(\theta)^2} \sin(\theta - \phi_2) \right] d\theta \end{aligned} \quad (3.43)$$

which is not positive definite for all (a, b) combinations. It fails to do so, when the function inside the brackets, $[\dots]$, becomes negative. Restricting to $a, b \in \mathbb{R}$, the condition simplifies as the gap opens about $\theta = 0$

$$\begin{aligned} 1 - ar(0) - \frac{b}{r(0)} &\leq 0 \\ \Rightarrow \exp \left(ar(0) + \frac{b}{r(0)} \right) &\geq e. \end{aligned} \quad (3.44)$$

From Eq. (3.23) $r(0)$ is given by

$$r(0) = \exp \left(ar(0) - \frac{b}{r(0)} \right). \quad (3.45)$$

The phase diagram of the model is shown in Fig. 10.

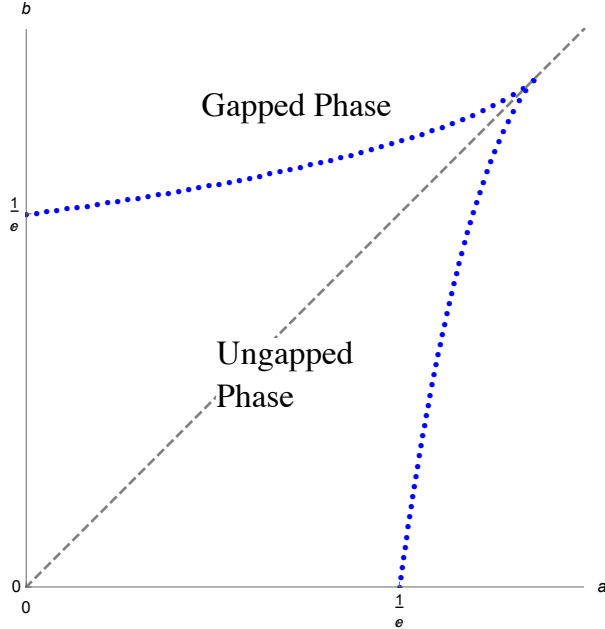


Figure 10: The phase diagram of the ab -model in the a - b plane.

It would be interesting to know how quantities change across the gap opening transition and also the order of the phase transition. To study that we first restrict ourselves to a special case, $b = 0$ in our model. Then from Eqs. (3.44) and (3.45) the gap opens about $a = \frac{1}{e}$, $R = e$, and since the ungapped phase has no branch cuts in the eigenvalue distributions, ϕ should start from zero, about the gap-opening point. And the conditions Eqs. (3.36) and (3.37) simplifies to

$$aR \left(\frac{\cos(\phi) + 1}{2} \right) = 1 \quad (3.46)$$

and Eq. (3.39) to

$$\left(\frac{1 - \cos(\phi)}{2} \right) \ln \left(\frac{1 - \cos(\phi)}{2} \right) = \left(\frac{1 + \cos(\phi)}{2} \right) \ln \left(\frac{R}{e} \right). \quad (3.47)$$

The observable $\langle \text{Tr} (U) \rangle$ becomes

$$\begin{aligned} \langle \text{Tr} (U) \rangle &= 0 && \text{(Ungapped)} \\ &= \left(\frac{a(\cos(\phi)^2 - 1)R^2}{4} \right) && \text{(Gapped)} \end{aligned} \quad (3.48)$$

Since the first derivative of free-energy $F[a]$ given by

$$\frac{\partial F[a]}{\partial a} = \frac{\partial \ln Z[a]}{\partial a} = \frac{1}{Z[a]} \int [DU] \text{Tr} (U) \exp(a \text{Tr} (U)) = \langle \text{Tr} (U) \rangle \quad (3.49)$$

is the expectation value of $\text{Tr} (U)$, we find that it is continuous across the gap.

Upon expanding about

$$a = \frac{1}{e} + \delta a, \quad \cos(\phi) = 1 - 2\delta p \text{ and } R = e + \delta R \quad (3.50)$$

the variation of $\delta \langle \text{Tr} (U) \rangle$ is given by

$$\delta \langle \text{Tr} (U) \rangle = \delta \left(\frac{a(\cos(\phi)^2 - 1)R^2}{4} \right) = -e\delta p. \quad (3.51)$$

From Eqs. (3.46) and (3.47) we get

$$\delta p = e\delta a + \frac{\delta R}{e}, \quad (3.52)$$

and

$$\delta p \ln(\delta p) = \frac{\delta R}{e}. \quad (3.53)$$

Eliminating δR from above two equations we get the equation

$$\delta p(1 - \ln(\delta p)) = e\delta a. \quad (3.54)$$

To invert the above equation let us substitute $\delta p \rightarrow e^k$. Then we have

$$(k-1)e^{(k-1)} = -\delta a. \quad (3.55)$$

The above equation is of the form, $xe^x = y$, which can be inverted to express x as a function of y and it is known as the Lambert-W function [37]. (It is often expressed as $W_c(y)$.) This function is in general a multivalued-complex function, where $c \in \mathbf{Z}$, chooses each branch. Since $\delta a > 0$ and $\delta p \in \mathbf{R}$ we have two real valued branches: $W_0(y)$ (the principal branch) and $W_{-1}(y)$.

Therefore,

$$\delta p = e^{W_0(-\delta a)+1} \text{ or } e^{W_{-1}(-\delta a)+1}. \quad (3.56)$$

For small values of δa we know that

$$\lim_{\delta a \rightarrow 0} W_0(-\delta a) = 0, \quad \lim_{\delta a \rightarrow 0} W_{-1}(-\delta a) \approx \ln(\delta a). \quad (3.57)$$

Therefore, δp will vanish as $\delta a \rightarrow 0$ only if we choose the second branch, i.e., $\delta p = e^{W_{-1}(-\delta a)+1}$. Hence

$$\delta \langle \text{Tr} (U) \rangle = -e^{W_{-1}(-\delta a)+2}. \quad (3.58)$$

Now the second derivative of free energy

$$\frac{\partial^2 F}{\partial(\delta a)^2} = \frac{\partial(\delta \langle \text{Tr} (U) \rangle)}{\partial(\delta a)} \frac{e^2}{W_{-1}(-\delta a) + 1} \quad (3.59)$$

goes to zero as $\delta a \rightarrow 0$ and is continuous across the gap. But the third derivative

$$\frac{\partial^3 F}{\partial(\delta a)^3} = -\frac{e^2 W_{-1}(-\delta a)}{\delta a (W_{-1}(-\delta a) + 1)^3} \quad (3.60)$$

diverges as $\delta a \rightarrow 0$. Hence it has a third order phase transition. It can also be shown that similar arguments hold in the generic case $b \neq 0$. Thus we conclude that the ab -Model displays a third order phase transition.

4 Gauge Theory to Unitary Matrix Model

A unitary matrix model arises in a one-loop formulation of QCD (and analogous $SU(N)$ gauge theories) on compact spaces (often $S^1 \times S^3$). This was originally derived in [38–41] for theories with more general matter content.

The one-loop effective action of QCD on $S^1 \times S^3$ with chemical potential μ and quark mass m has the form [26], with thermal Polyakov loop as the unitary matrix model

$$S = \sum_{n=1}^{\infty} \frac{1}{n} z_b \left(\frac{n\beta}{R} \right) \text{Tr} U^n \text{Tr} U^{\dagger n} + \sum_{n=1}^{\infty} \frac{(-1)^n}{n} N_f z_f \left(\frac{n\beta}{R}, mR \right) \left[e^{n\beta\mu} \text{Tr} U^n + e^{-n\beta\mu} \text{Tr} U^{\dagger n} \right]. \quad (4.1)$$

The quadratic term in Polyakov loop is the contribution from adjoint fields and the linear term is the contribution from the fundamental matter fields. Here, we have taken the adjoint contribution to be bosonic and the contribution from fundamental fields to be fermionic.

To be noted is that in the free theory the effective action is determined in terms of single particle partition function

$$z_b\left(\frac{\beta}{R}\right) = 2 \sum_{l=1}^{\infty} l(l+2)e^{-\beta(l+1)/R}, \quad (4.2)$$

and

$$z_f\left(\frac{\beta}{R}, mR\right) = 2 \sum_{l=1}^{\infty} l(l+1)e^{-\frac{\beta}{R}\sqrt{(l+\frac{1}{2})^2+m^2R^2}}. \quad (4.3)$$

In the above equations R is the radius of S^3 . We use dimensionless variables β/R , μR and mR in numerical simulations.

An analogous action, for the simpler 0 + 1 dimensional case would be,

$$\begin{aligned} z_b &= 0, \\ z_f &= 2e^{-\beta m}, \end{aligned} \quad (4.4)$$

where the parameter m is the mass of the fundamental fermions.

In the low temperature limit, $\beta \rightarrow \infty$, we have $z_b(\infty) = 0$ and so the gluonic contribution is negligible. Thus the action is

$$S = S_{\text{Vdm}} + S_f, \quad (4.6)$$

where S_f is the fundamental fermionic contribution. The fermionic part could be summed in a logarithm

$$S[U] = - \sum_{l=1}^{\infty} \sigma_l \left(\log \left[\det \left(1 + e^{\beta(\mu - \epsilon_l)} U \right) \det \left(1 + e^{\beta(-\mu - \epsilon_l)} U^{-1} \right) \right] \right). \quad (4.7)$$

4.1 Observables

We can study several interesting observables in the model described above. We briefly describe them below

1. The most natural set of observables are Polyakov line and inverse Polyakov line.
3. Fermion number f_N

It gives the number of fermions minus the number of anti-fermions in a given volume

$$f_N = \frac{1}{\beta} \left(\frac{\partial \log Z}{\partial \mu} \right). \quad (4.8)$$

In the model we study here we have a single chemical potential μ . In general there can be chemical potential for each fermion flavor.

The quark number susceptibility χ_f measures the response of the fermion number density to infinitesimal changes in the chemical potential,

$$\chi_f = \frac{1}{\beta} \frac{\partial f_N}{\partial \mu}. \quad (4.9)$$

This observable follows the behavior of the Polyakov line. Thus, it also serves as an indicator of confinement-deconfinement transitions for nonzero chemical potential.

4. Pressure p

$$p = \frac{1}{\beta} \left(\frac{\partial \log Z}{\partial V_3} \right), \quad (4.10)$$

with V_3 denoting the spatial volume.

5. Energy E

It can be constructed from pressure and fermion number density

$$E = -pV_3 + \mu f_N. \quad (4.11)$$

It is also possible to compute the chiral condensate and average phase, though we will not compute them in this work. The chiral condensate $\langle \bar{\psi}\psi \rangle$ is given by

$$\langle \bar{\psi}\psi \rangle = -\frac{1}{\beta V_3} \lim_{m \rightarrow 0} \left(\frac{\partial \log Z}{\partial m} \right), \quad (4.12)$$

and the average phase $\langle e^{i\phi} \rangle_{pq}$ has the form

$$\langle e^{i\phi} \rangle_{pq} = \frac{Z}{Z_{pq}}, \quad (4.13)$$

where pq refers to the phase quenched theory.

4.2 Single Level Model with Positive Chemical Potential

We can truncate the action given in Eq. (4.7) in a double scaling limit:

$$\begin{aligned} \beta &\rightarrow \infty, \\ \mu &\rightarrow \epsilon_0, \\ \exp(\beta(\mu - \epsilon_l)) &= \xi, \end{aligned} \quad (4.14)$$

where ϵ_0 is a fixed quark energy level and ξ the effective fugacity.

Only contribution from a single level survives here,

$$S[U] = -\sigma \log(1 + \xi U). \quad (4.15)$$

The effective action on the angle variables include the Vandermonde piece and a Lagrange multiplier.

In the large N limit, the integral over the angles is dominated by a saddle point obtained by solving the equation of motion that follows from the effective action involving Eq. (4.15)

$$\frac{\partial S}{\partial \theta_i} = iN\mathcal{N} - \frac{iN\sigma\xi e^{i\theta}}{(1 + \xi e^{i\theta_i})} - \sum_{j(\neq i)}^N \cot\left(\frac{\theta_i - \theta_j}{2}\right). \quad (4.16)$$

Here also the action is not hermitian, giving rise to the *sign problem* in the presence of a chemical potential. As a result the saddle point configuration will lie out in the complex plane. If we define $z_i = \exp(i\theta_i)$ then in the presence of the non-real potential the z_i will move off the unit circle in the z -plane.

We can explore the nature of eigenvalue distribution on the complex plane for various values of effective fugacity ξ . We find that when ξ is either very small or large, the potential vanishes and so we expect the $\{z_i\}$ to be uniformly distributed around the unit circle. Thus, when μ varies from $\mu \ll \epsilon$ to $\mu \gg \epsilon$ the quark energy level becomes occupied and the effective fermion number jumps by factor σ . In Ref. [26] the authors provide a detailed description of this transition.

Let us look at the various regimes of ξ and see how it affects the eigenvalue distribution, following the analytical study given in Ref. [26].

1. *The small ξ confined phase*

In the small ξ confining phase the effective fermion number vanishes, $\mathcal{N} = 0$, and the Polyakov line expectation values are

$$P = 0, \quad P^{-1} = \sigma\xi. \quad (4.17)$$

Thus we have $P \neq P^{-1}$, as a result of the complex action.

As ξ is increased the contour of eigenvalue distribution opens into an arc, just as the matrix model solved by Gross and Witten [27] and Wadia [28, 29].

The line of phase transitions in the (μ, T) plane corresponds to the straight line

$$\mu = \epsilon - T \left[(1 + \sigma) \log(1 + \sigma) - \sigma \log \sigma \right]. \quad (4.18)$$

Note that this approximation is valid only in the low temperature ($\beta \rightarrow \infty$) limit.

2. *The large ξ confined phase*

In this phase the effective fermion number is

$$\mathcal{N} = \sigma, \quad (4.19)$$

indicating that the level is now occupied.

The Polyakov line expectation values are

$$P = \frac{\sigma}{\xi}, \quad P^{-1} = 0. \quad (4.20)$$

Comparing with the previous case the behavior of P and P^{-1} swaps over along the replacement $\xi \rightarrow \xi^{-1}$.

The large ξ confined phase persists until the value

$$\xi = \xi_2 = \frac{(1 + \sigma)^{1+\sigma}}{\sigma^\sigma}. \quad (4.21)$$

For smaller values of ξ the contour of eigenvalue distribution is not closed and the phase does not exist. The points of transition $\xi = \xi_1$ and $\xi = \xi_2$ satisfy $\xi_1 \xi_2 = 1$.

In the (μ, T) plane the boundary lies along the straight line

$$\mu = \epsilon + T \left[(1 + \sigma) \log(1 + \sigma) - \sigma \log \sigma \right], \quad (4.22)$$

again valid in the low temperature limit.

3. The deconfined phase

In the region $\xi_1 \leq \xi \leq \xi_2$, experience with GWW matrix model suggests that the eigenvalue distribution exhibits the shape of an open contour.

In this regime we get a condition

$$\xi = \frac{(\sigma - \mathcal{N})^{\sigma - \mathcal{N}} (1 + \mathcal{N})^{1 + \mathcal{N}}}{\mathcal{N}^{\mathcal{N}} (1 + \sigma - \mathcal{N})^{1 + \sigma - \mathcal{N}}}. \quad (4.23)$$

This equation determines \mathcal{N} as a function of ξ .

From the above equation it follows that across the transitions at $\xi = \xi_1$ and $\xi = \xi_2$, fermion number density \mathcal{N} and its first derivative $\frac{\partial \mathcal{N}}{\partial \mu}$ are continuous, however higher derivatives are discontinuous. Since \mathcal{N} is the effective fermion number, the first derivative of the grand potential, it follows that the transitions are third order, just as in the original GWW model.

For a single winding, the Polyakov lines are

$$P = \frac{\mathcal{N}}{\sigma + 1 - \mathcal{N}} \frac{1}{\xi}, \quad P^{-1} = \frac{\sigma - \mathcal{N}}{1 + \mathcal{N}} \xi. \quad (4.24)$$

Using complex Langevin dynamics we have simulated the single level matrix model. In Fig. 11 we show the eigenvalue distributions of the Polyakov line in the confined and deconfined phases as a function of the logarithm of the effective fugacity, $\log \xi$, for $SU(N)$ case with $N = N_f = 500$, quark mass $m = 0$ and inverse temperature $\beta = 30$ (low T). We see that the eigenvalue distributions start with a closed contour (confined phase), passes through an open contour (deconfined phase) and again goes into a closed contour. (This figure can be compared with Fig. 12 in Sec. 4.1 of Ref. [26], where it was obtained through analytical methods.)

In Fig. 12 we provide the (normalized) effective fermion number $\langle f_N \rangle$, and in Fig. 13 the Polyakov line expectation value $\langle P \rangle$ and the inverse Polyakov line expectation value $\langle P^{-1} \rangle$

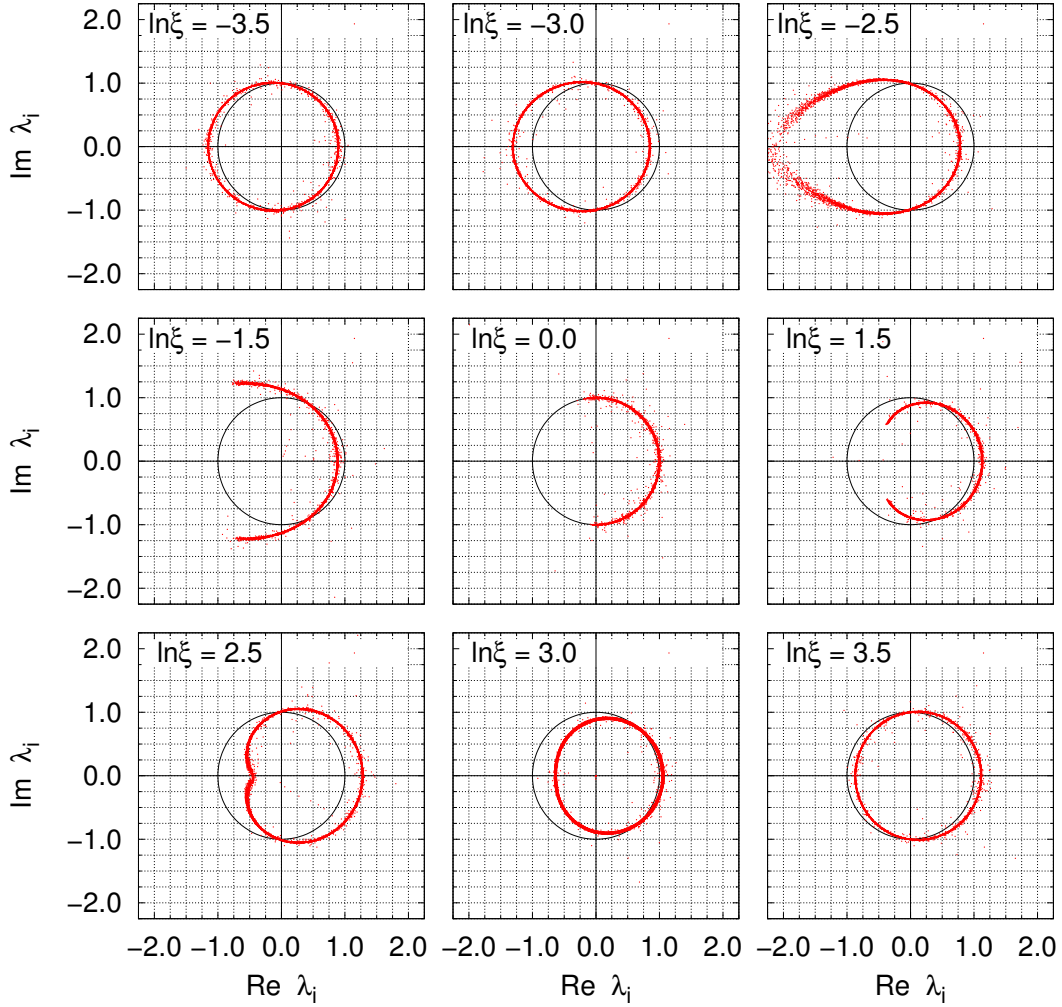


Figure 11: The eigenvalue distribution in the confined and deconfined phases as a function of the logarithm of the effective fugacity, $\log \xi$, for single-level $SU(N)$ matrix model with $N = N_f = 500$, quark mass $m = 0$ and inverse temperature $\beta = 30$ (low T). The data are obtained through complex Langevin simulations with Langevin time step $\Delta\tau = 0.000005$, thermalization steps $N_{\text{therm}} = 18000$, generation steps $N_{\text{gen}} = 2000$ and with measurements performed every 100 steps. The solid unit circles are guide to the eye.

across a pair of GWW transitions from the small ξ confined phase through the deconfined phase to the large ξ confined phase. The transitions from confined/deconfined phases occur when either $\langle P \rangle$ or $\langle P^{-1} \rangle$ vanish. The parameters used are: $N = N_f = 3$ and 500 , quark mass $m = 0$ and inverse temperature $\beta = 30$. The simulations show excellent agreement with the analytical results in the large N .

In Figs. 14 and 15 we show the Polyakov lines and fermion number density for a range of simulation parameters: $\beta = \{10, 15, \dots, 100\}$ and $\mu = \{3.0, 3.025, 3.05, \dots, 4.0\}$. The quark energy level of the model is fixed to $\epsilon = 3.5$ corresponding to the third level. The Polyakov loops peak around $\mu = 3.5$. In Fig. 14 we show the behavior of Polyakov and inverse Polyakov loops for $\beta = \{25, 50, 75, 100\}$. It is clear that the widths of the Polyakov

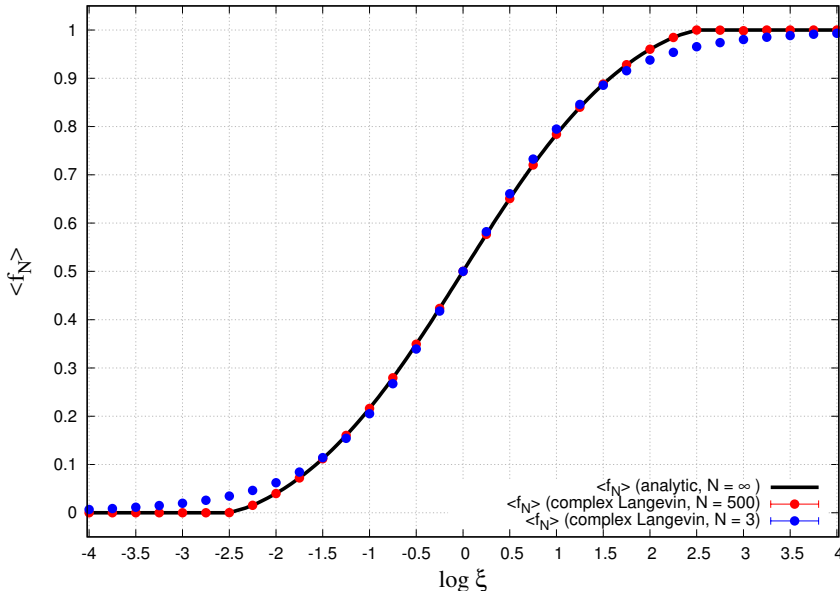


Figure 12: The (normalized) effective fermion number $\langle f_N \rangle$ across the pair of GWW transitions from the small ξ confined phase through the deconfined phase to the large ξ confined phase. The solid curve is the analytical result ($N = \infty$). The data points are obtained through complex Langevin simulations. We used Langevin time step $\Delta\tau = 0.000005$, thermalization steps $N_{\text{therm}} = 10000$, generation steps $N_{\text{gen}} = 10000$ and with measurements performed every 100 steps. Here red data points are for $N = N_f = 500$ and blue data points are for $N = N_f = 3$. We used quark mass $m = 0$ and inverse temperature $\beta = 30$ (low T).

loops decrease as the temperature is reduced (large β) and the behavior of inverse Polyakov line precedes that of the Polyakov line as a function of μ . In Fig. 15 we show the behavior of the (normalized) fermion number density $\langle f_N \rangle$ as a function of chemical potential and inverse temperature. The transition in fermion number becomes sharper as the temperature is decreased (high β). The model is in a deconfined phase when $0 < \langle f_N \rangle < 1$.

When the quark mass is non-vanishing in QCD, the expectation values of bulk observables such as the fermion number density, Polyakov lines and energy, exhibit the ‘Silver Blaze’ behavior. The bulk observables are nearly zero until onset [42] to a deconfinement transition, which occurs when the chemical potential increases to the value of the lightest quark mass. In our model the onset occurs at $\mu = m$. In Fig. 16 (Left) we show the effective fermion number density as a function of chemical potential for large quark mass, near the onset $\mu = m = 25$ for $N = N_f = 100$ and $\beta = 25$ (low T). The Polyakov line as a function of chemical potential is given in Fig. 16 (Right). In the large m limit, similar to the $m = 0$ case, the behavior of inverse Polyakov line $\langle P^{-1} \rangle$ precedes that of $\langle P \rangle$ as a function of μ . The transition in μ occurs around onset at m .

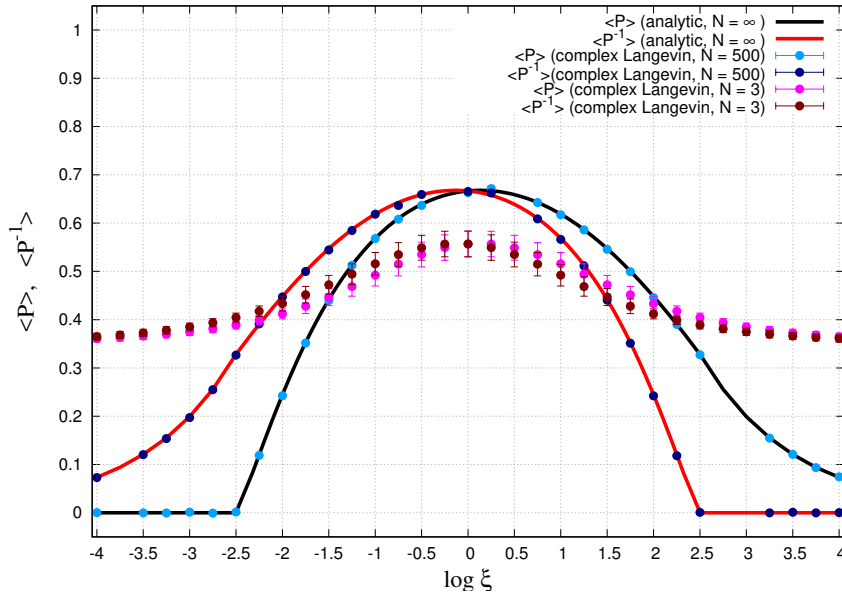


Figure 13: The Polyakov line $\langle P \rangle$ and inverse Polyakov line $\langle P^{-1} \rangle$ across the pair of GWW transitions from the small ξ confined phase through the deconfined phase to the large ξ confined phase. The transitions from confined/deconfined phases occur when either $\langle P \rangle$ or $\langle P^{-1} \rangle$ vanish. The solid curves are the analytical results ($N = \infty$). The data points are obtained through complex Langevin simulations. We used Langevin time step $\Delta\tau = 0.000005$, thermalization steps $N_{\text{therm}} = 10000$, generation steps $N_{\text{gen}} = 10000$ and with measurements performed every 100 steps. We simulated the model with $N = N_f = 500$ and $N = N_f = 3$. We used quark mass $m = 0$ and inverse temperature $\beta = 30$ (low T).

4.3 Single Level Model with Two Fugacities

In this section we consider the phase diagram of the model given by the action with two effective fugacities

$$S[U] = -\sigma \left[\log \left(1 + \xi_1 U \right) + \log \left(1 + \xi_2 U^\dagger \right) \right], \quad (4.25)$$

where

$$\begin{aligned} \xi_1 &= e^{\beta(\mu - \epsilon)}, \\ \xi_2 &= e^{\beta(-\mu - \epsilon)}. \end{aligned} \quad (4.26)$$

Such a model naturally arises from 0 + 1-dimensional gauge theory with a fundamental fermion.

In Fig. 17 we provide the phase diagram of this model on the (μ, β) plane for the level $l = 1$. (Corresponding to quark energy level $\epsilon = 1.5$ and $\sigma = 4$.) From the behavior of the expectation value of the fermion number density we see that the phase transition from confined to deconfined phase is smooth on the (μ, β) plane even at high temperature ($0.1 \leq \beta \leq 2.0$).

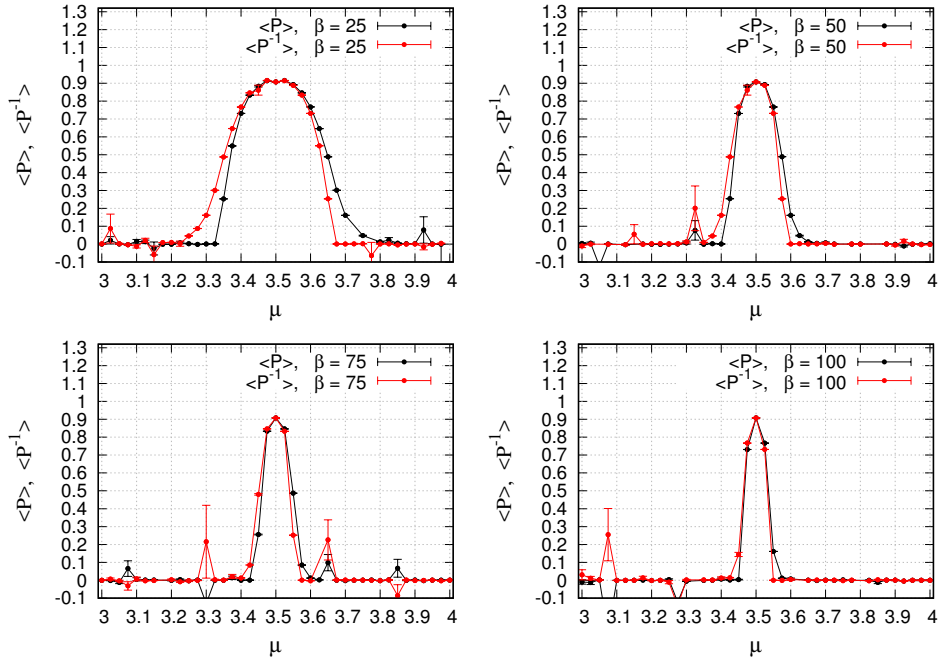


Figure 14: Polyakov line $\langle P \rangle$ and inverse Polyakov line $\langle P^{-1} \rangle$ as a function of chemical potential for single level matrix model with quark energy level $\epsilon = 3.5$ and quark mass $m = 0$. Here $N = N_f = 500$ and $\beta = 25, 50, 75, 100$. The data are obtained through complex Langevin simulations with Langevin time step $\Delta\tau = 0.000005$, thermalization steps $N_{\text{therm}} = 5000$, generation steps $N_{\text{gen}} = 5000$ and with measurements performed every 50 steps.

4.4 Single Level Model with Interaction

It would be interesting to consider the single-level matrix model with a non-trivial interaction turned on. We take a Polyakov line interaction term of the form

$$S_{\text{int}}[U] = g (\text{Tr } U)(\text{Tr } U^{-1}). \quad (4.27)$$

Here g denotes a coupling parameter.

Thus we have

$$S[U] = -\sigma \log \left(1 + e^{\beta(\mu - \epsilon)} U \right) + S_{\text{int}}[U]. \quad (4.28)$$

Here also we take the quark energy level to be fixed at $\epsilon = 3.5$. The action is again not hermitian, giving rise to the sign problem in the presence of a chemical potential. In Figs. 18 and 19 we plot the fermion number density and the Polyakov lines of the interacting model for various values of the coupling $g = 0, 5, 20, 100$. It is evident that the confinement/deconfinement transition becomes sharper as the interaction strength is increased. The behavior of the Polyakov lines show that the model is in a confined phase for most of the values of the chemical potential.

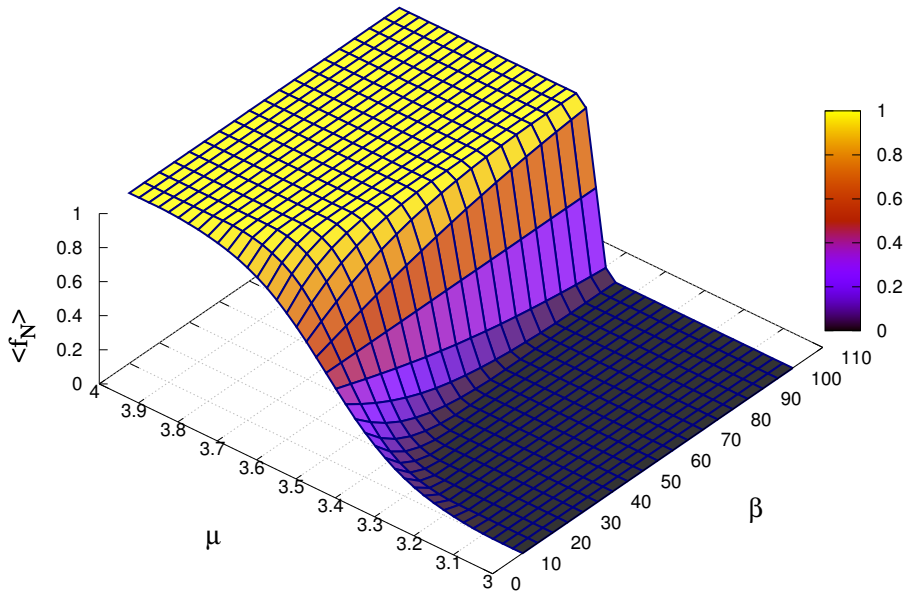


Figure 15: The (normalized) fermion number density $\langle f_N \rangle$ as a function of chemical potential μ and inverse temperature β for single-level matrix model with quark energy level $\epsilon = 3.5$ and quark mass $m = 0$. Here $N = N_f = 500$. The model is in a deconfined phase when $0 < \langle f_N \rangle < 1$. The data are obtained through complex Langevin simulations with Langevin time step $\Delta\tau = 0.000005$, thermalization steps $N_{\text{therm}} = 5000$, generation steps $N_{\text{gen}} = 5000$ and with measurements performed every 50 steps.

5 Conclusions and Discussions

In this work we have successfully used complex Langevin dynamics with stochastic quantization to simulate the thermodynamics of a large N unitary matrix models with complex actions. We started with a simple matrix model called the *ab*-model and investigated its phase structure analytically and numerically. The numerical simulations show excellent match with analytical results. We also studied a model obtained from the effective theory of QCD on $S^1 \times S^3$ at low temperature and finite quark chemical potential. At zero quark mass and low temperature our simulations showed a series of GWW confinement-deconfinement phase transitions as a function of the chemical potential. The phases are characterized by the distribution of eigenvalues of the Polyakov line on the complex plane. In the large quark mass regime we were also able to observe the Silver Blaze behavior in that the bulk observables are roughly zero until the onset transition to the deconfined phase, which occurs at $\mu = m$. We also simulated the model with a simple non-trivial Polyakov line interaction turned on. The model prefers to live in the confined phase as the interaction strength is increased.

We also note that each confinement-deconfinement transition in the Polyakov line is associated with a quark energy level transition. It is interesting to note that the non-monotonic behavior of Polyakov lines have been observed in lattice simulations of QCD

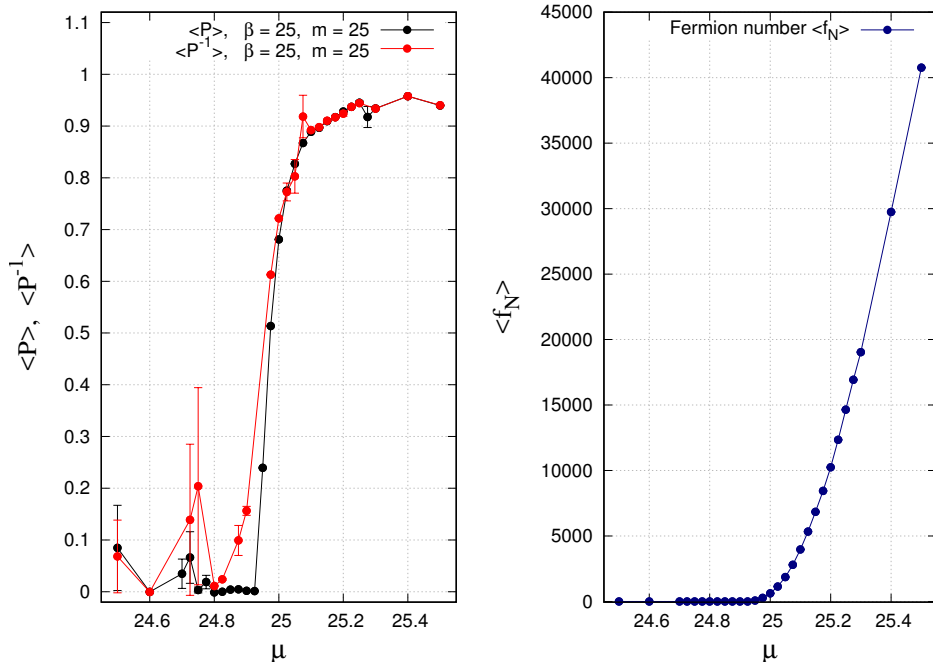


Figure 16: The Silver Blaze behavior of observables $\langle f_N \rangle$, $\langle P \rangle$ and $\langle P^{-1} \rangle$ at non-zero quark mass m . (Left) Polyakov line $\langle P \rangle$ and inverse Polyakov line $\langle P^{-1} \rangle$ and (Right) fermion number $\langle f_N \rangle$ as a function of chemical potential for large quark mass near onset at $\mu = m = 25$. Here $N = N_f = 100$ and $\beta = 25$ (low T). The data are obtained through complex Langevin simulations with Langevin time step $\Delta\tau = 0.00005$, thermalization steps $N_{\text{therm}} = 5000$, generation steps $N_{\text{gen}} = 5000$ and with measurements performed every 50 steps.

with gauge group $SU(2)$ near its saturation density in Ref. [43].

We successfully applied complex Langevin dynamics to QCD on $S^1 \times S^3$ with finite chemical potential and computed several bulk observables. We provided our simulation results on this in Appendix A.

There are several interesting future directions. One could consider complex Langevin simulations of the model with several quark flavors with masses m_f and different chemical potentials μ_f . One could also add other types of non-trivial interaction terms into the model and look for cross-over transitions on the (μ, β) plane [44]. It would also be interesting to see if there exists an AdS/CFT type gravitational dual of the models we studied here. One could ask the question whether the infinite sequence of GWW transitions that we observe in the matrix model be seen in the dual gravitational description.

Acknowledgments

We gratefully acknowledge support from the International Centre for Theoretical Sciences (ICTS-TIFR), the Infosys Foundation and the Indo-French Centre for the Promotion of Advanced Research (IFCPAR/CEFIPRA). We thank Spenta Wadia, Takehiro Azuma and Jun Nishimura for a careful reading of our manuscript and providing valuable suggestions. We also thank Andrei Alexandru, Gautam Mandal, Antonio Gonzalez-Arroyo, and Shiraz

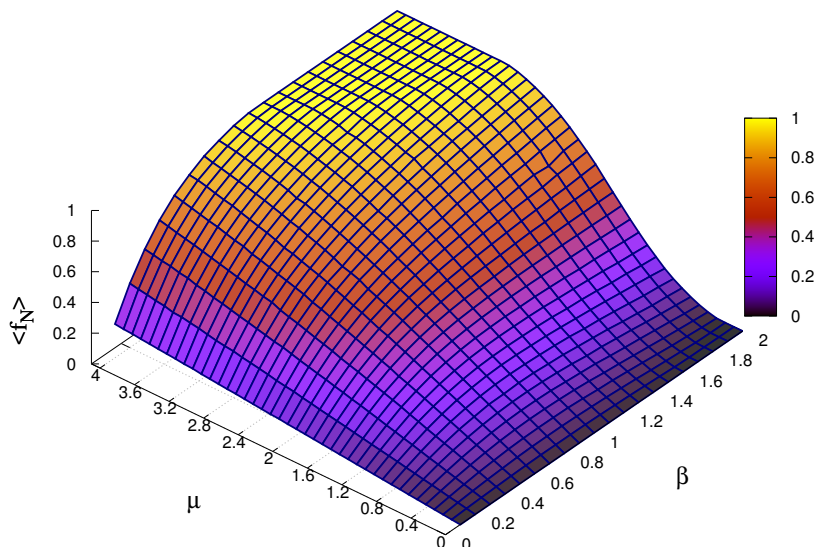


Figure 17: The (normalized) fermion number density $\langle f_N \rangle$ as a function of chemical potential μ and inverse temperature β for the matrix model with two effective fugacities. The model has fixed quark energy level $\epsilon = 1.5$, quark mass $m = 0$ and $N = N_f = 100$. The model is in a deconfined phase when $0 < \langle f_N \rangle < 1$. The data are obtained through complex Langevin simulations with Langevin time step $\Delta\tau = 0.00005$, thermalization steps $N_{\text{therm}} = 10000$, generation steps $N_{\text{gen}} = 50000$ and with measurements performed every 100 steps.

Minwalla for valuable comments and discussions. We also thank the organizers of ICTS program “Nonperturbative and Numerical Approaches to Quantum Gravity, String Theory and Holography”, 2018, where this work was presented. PB thanks TIFR theory group for inviting him to present this work as a part of the Quantum Spacetime Seminars.

A QCD on $S^1 \times S^3$ at Finite Chemical Potential

In this section we discuss the results obtained through complex Langevin simulations of QCD on $S^1 \times S^3$ with finite chemical potential, zero quark mass and at low temperature, given by the action Eq. (4.7).

A.1 Fermion number $\langle f_N \rangle$

In Fig. 21 we show $\langle f_N \rangle$ as a function of μ for low temperatures for $m = 0$. The presence of an occupation level structure is evident. The transitions occur when $\epsilon_l - \mu$ changes sign, that is, when μ passes a quark energy level.

It is interesting to compare with the results obtained in Ref. [26]. We also note that in Ref. [45] Banerjee and Chandrasekharan observed the same level structure in the particle number in the non-linear $O(2)$ sigma model.

The fermion number can be used as an order parameter of the confinement-deconfinement transitions in the large N theory. The first and second derivatives of the grand potential,

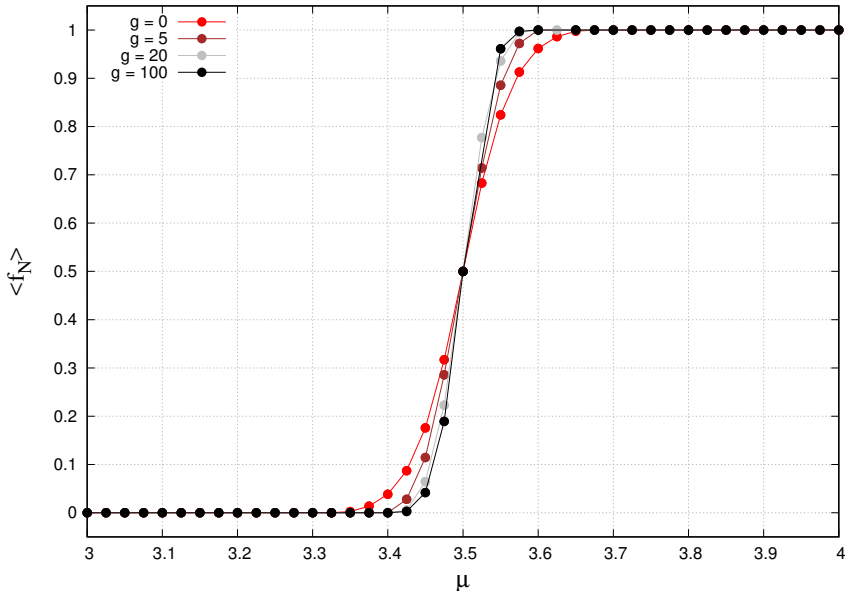


Figure 18: The (normalized) fermion number density $\langle f_N \rangle$ as a function of chemical potential μ for interacting single-level matrix model with couplings $g = 0, 5, 20, 100$. We take the quark energy level $\epsilon = 3.5$ and quark mass $m = 0$. Here $N = N_f = 500$. The data are obtained through complex Langevin simulations with Langevin time step $\Delta\tau = 0.000005$, thermalization steps $N_{\text{therm}} = 5000$, generation steps $N_{\text{gen}} = 5000$ and with measurements performed after every 50 steps. The model is in a deconfined phase when $0 < \langle f_n \rangle < 1$. The data show that the phase transition becomes sharper as the interaction strength g is increased.

$\langle f_N \rangle$ and $\langle \partial f_N / \partial \mu \rangle$ are continuous as a function of the chemical potential but the third derivative $\langle \partial^2 f_N / \partial \mu^2 \rangle$ is discontinuous. This indicates that the transitions are third order, of the GWW type.

A.2 Polyakov Lines $\langle P \rangle$ and $\langle P^{-1} \rangle$

When the chemical potential is zero the Polyakov line $\langle P \rangle$ and the conjugate Polyakov line $\langle P^{-1} \rangle$ coincide and it is no longer the case for non-zero chemical potential. In Fig. 21 we show $\langle P \rangle$ and $\langle P^{-1} \rangle$ as a function of μ . Each spike in $\langle P \rangle$ and $\langle P^{-1} \rangle$ corresponds to a level transition in $\langle f_N \rangle$. They exhibit similar behavior as a function of μ however, the behavior of $\langle P^{-1} \rangle$ always precedes that of $\langle P \rangle$ at the start and finish of each level transition. We note that the lines peak at $\mu = 1.5, 2.5, \dots$. We also note that the widths of deconfined regions increase as μ is increased.

A.3 Pressure $\langle p \rangle$ and Energy $\langle E \rangle$

In Figs. 22 and 23 we provide the pressure multiplied by the 4-volume and energy $\langle E \rangle = -\langle p \rangle + \mu \langle f_N \rangle$. We note that the pressure exhibits a level structure. The energy levels are not horizontal. The factor μ in front of the fermion number causes the levels to rise linearly with μ .

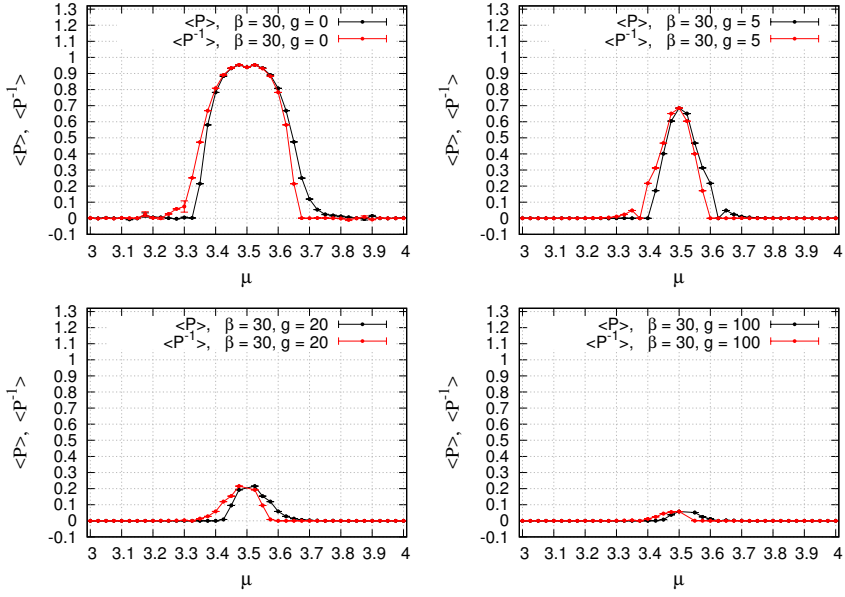


Figure 19: The Polyakov line and inverse Polyakov line across a pair of GWW transitions for the interacting single-level matrix model with a fixed quark energy level $\epsilon = 3.5$, quark mass $m = 0$ and $N = N_f = 500$. The data are obtained through complex Langevin simulations with Langevin time step $\Delta\tau = 0.000005$, thermalization steps $N_{\text{therm}} = 5000$, generation steps $N_{\text{gen}} = 5000$ and with measurements performed after every 50 steps. The solid lines are guide to the eye. The plots indicate that the model prefers to stay in a confined phase as the interaction strength g is increased.

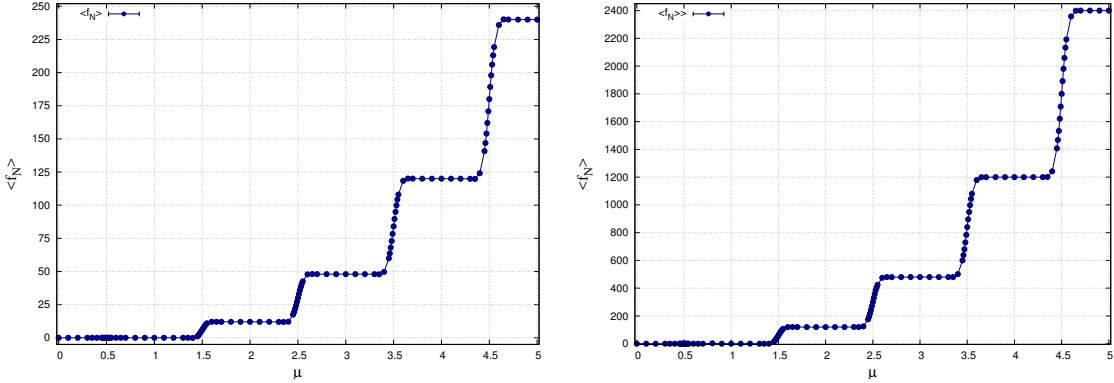


Figure 20: Expectation values of the effective fermion number $\langle f_N \rangle$ as a function of the quark chemical potential for QCD on $S^1 \times S^3$. Here $m = 0$, inverse temperature $\beta = 30$, $N = N_f = 3$ (Left) and $N = N_f = 30$ (Right). The data are obtained through complex Langevin simulations with Langevin time step $\Delta\tau = 0.000005$, thermalization steps $N_{\text{therm}} = 10000$, generation steps $N_{\text{gen}} = 50000$ and with measurements performed every 100 steps. The solid lines are to guide the eye.

In Fig. 24 we show the eigenvalue distributions in the confined and deconfined phases as a function of the quark chemical for $N = N_f = 30$ and $\mu = 4.0, 4.5, 5.0$.

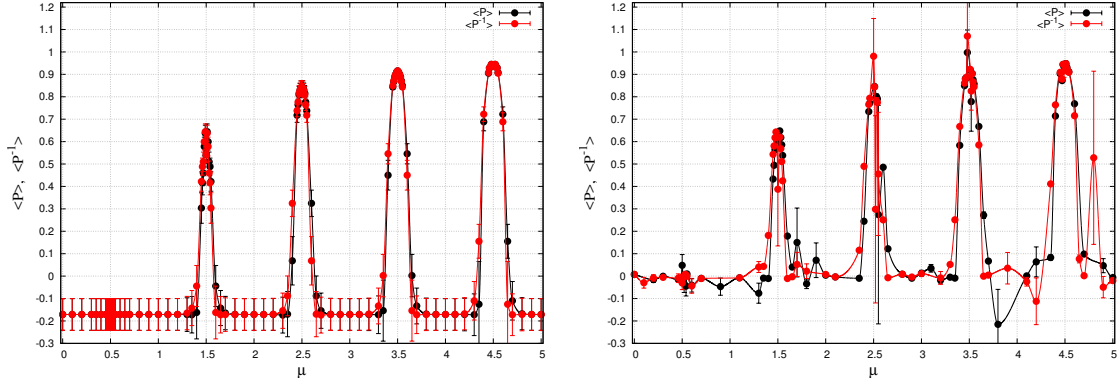


Figure 21: Expectation values of the Polyakov line $\langle P \rangle$ and inverse Polyakov line $\langle P^{-1} \rangle$ as a function of the quark chemical potential μ for QCD on $S^1 \times S^3$. Here $m = 0$, inverse temperature $\beta = 30$, $N = N_f = 3$ (Left) and $N = N_f = 30$ (Right). The data are obtained through complex Langevin simulations with Langevin time step $\Delta\tau = 0.00005$, thermalization steps $N_{\text{therm}} = 10000$, generation steps $N_{\text{gen}} = 50000$ and with measurements performed every 100 steps. The solid lines are to guide the eye.

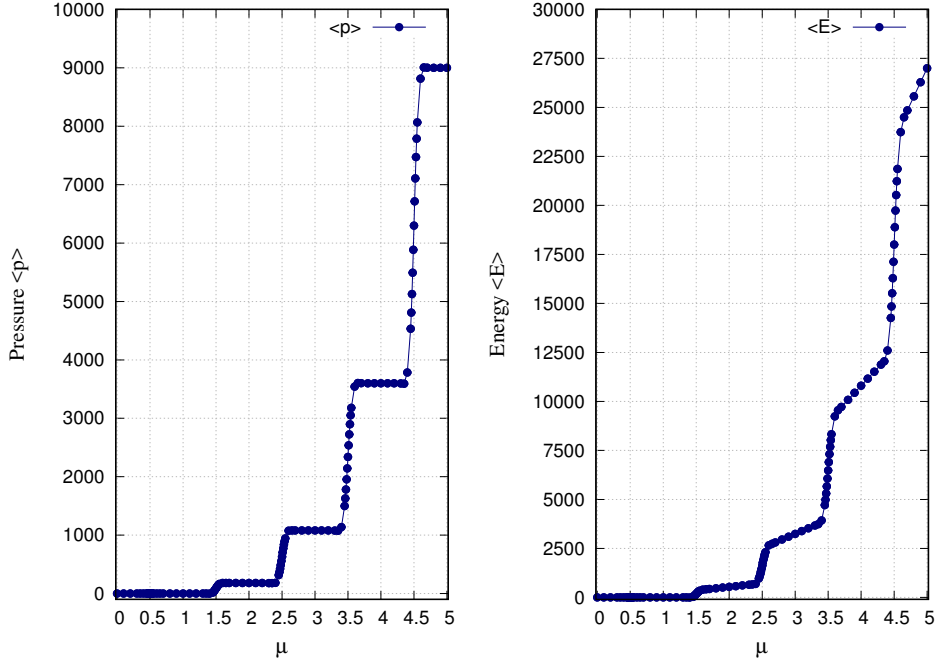


Figure 22: (Left) Pressure $\langle p \rangle$ and (Right) energy $\langle E \rangle$ as a function of the quark chemical potential for QCD on $S^1 \times S^3$. Here $N = N_f = 3$, $m = 0$ and inverse temperature $\beta = 30$. The data are obtained through complex Langevin simulations with Langevin time step $\Delta\tau = 0.00005$, thermalization steps $N_{\text{therm}} = 10000$, generation steps $N_{\text{gen}} = 50000$ and with measurements performed every 100 steps. The solid lines are guide to the eye.

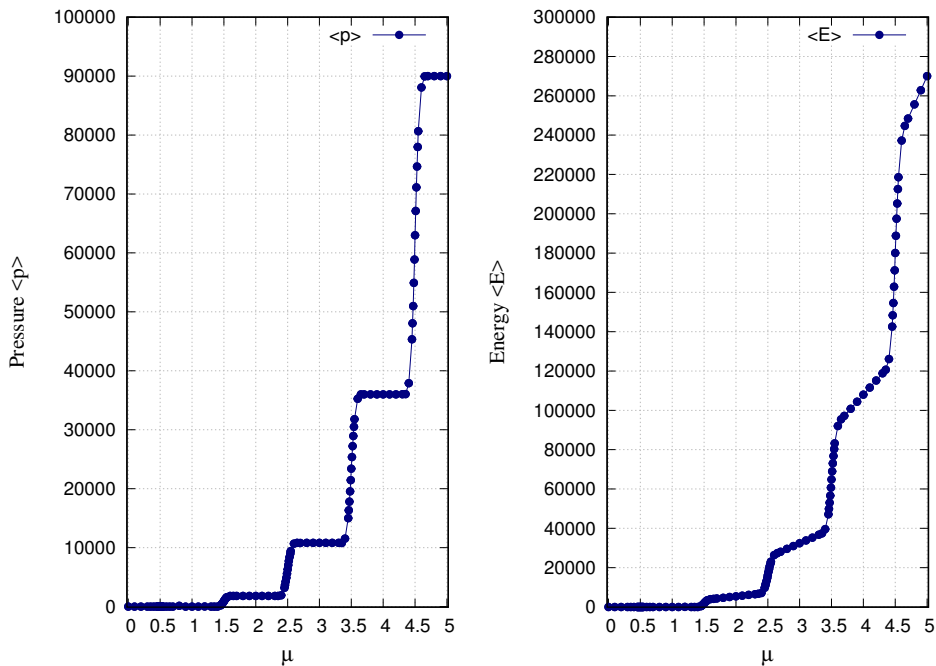


Figure 23: (Left) Pressure $\langle p \rangle$ and (Right) energy $\langle E \rangle$ as a function of the quark chemical potential for QCD on $S^1 \times S^3$. Here $N = N_f = 30$, $m = 0$ and inverse temperature $\beta = 30$. The data are obtained through complex Langevin simulations with Langevin time step $\Delta\tau = 0.00005$, thermalization steps $N_{\text{therm}} = 10000$, generation steps $N_{\text{gen}} = 50000$ and with measurements performed every 100 steps. The solid lines are guide to the eye.

B Reliability of Complex Langevin Dynamics

We would like to justify the use of complex Langevin dynamics for the matrix models we simulated in this work. In Ref. [46, 47] the authors suggested a possible criterion to determine the correct convergence of the complex Langevin method – the probability distribution of the magnitude of the drift term should fall off exponentially or faster. This criterion can, in general, be violated if the complexified fields develop large imaginary parts (the *excursion problem*). In Fig. 25 we show the probability distributions $P(u)$ for the magnitude of the drift term

$$u = \sqrt{\frac{1}{N^3} \sum_{i=1}^N \left| \frac{\partial S}{\partial \theta_i} \right|^2}, \quad (\text{B.1})$$

of the single level $SU(N)$ matrix model.

However, in our case the plots show that the probability distribution falls off like a power law with u . We also observed a similar behavior in the *ab*-model. One may speculate that the issue may be addressed by introducing an adaptive Langevin time step or an analytic re-definition of the variables. We think this needs further investigations.

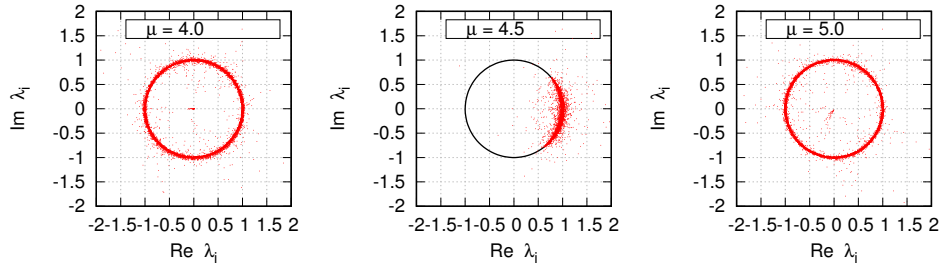


Figure 24: The eigenvalue distributions in the confined (Left and Right) and deconfined (Middle) phases as a function of the quark chemical potential for QCD on $S^1 \times S^3$. Here $N = N_f = 30$, $m = 0$ and inverse temperature $\beta = 30$. The data are obtained through complex Langevin simulations with Langevin time step $\Delta\tau = 0.00005$, thermalization steps $N_{\text{therm}} = 10000$, generation steps $N_{\text{gen}} = 50000$ and with measurements performed every 100 steps. The solid unit circles are guide to the eye.

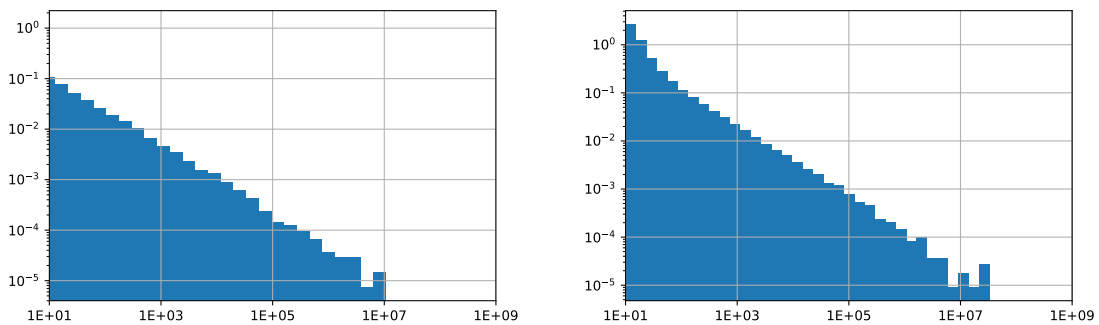


Figure 25: The probability distribution $P(u)$ of the magnitude of the drift term u for the single-level matrix model with positive chemical potential plotted in a log-log plot. (Left) The plot for the ungapped phase with an effective fugacity $\ln(\xi) = -3.5$. We find a power law decay with an exponent -1.53 . (Right) The plot for the gapped phase with an effective fugacity $\ln(\xi) = 1.5$. We find a power law decay with an exponent -1.67 . The Langevin evolution is performed for 600000 steps, without thermalization and with a Langevin step $\Delta\tau = 0.000005$. Here $N = N_f = 100$.

References

- [1] S. Muroya, A. Nakamura, C. Nonaka, and T. Takaishi, “Lattice QCD at finite density: An Introductory review,” *Prog. Theor. Phys.* **110** (2003) 615–668, [arXiv:hep-lat/0306031](https://arxiv.org/abs/hep-lat/0306031)

- [hep-lat].
- [2] P. de Forcrand, “Simulating QCD at finite density,” *PoS LAT2009* (2009) 010, [arXiv:1005.0539 \[hep-lat\]](#).
- [3] J. R. Klauder, “Coherent State Langevin Equations for Canonical Quantum Systems With Applications to the Quantized Hall Effect,” *Phys. Rev.* **A29** (1984) 2036–2047.
- [4] G. Parisi, “ON COMPLEX PROBABILITIES,” *Phys. Lett.* **131B** (1983) 393–395.
- [5] **AuroraScience** Collaboration, M. Cristoforetti, F. Di Renzo, and L. Scorzato, “New approach to the sign problem in quantum field theories: High density QCD on a Lefschetz thimble,” *Phys. Rev.* **D86** (2012) 074506, [arXiv:1205.3996 \[hep-lat\]](#).
- [6] H. Fujii, D. Honda, M. Kato, Y. Kikukawa, S. Komatsu, and T. Sano, “Hybrid Monte Carlo on Lefschetz thimbles - A study of the residual sign problem,” *JHEP* **10** (2013) 147, [arXiv:1309.4371 \[hep-lat\]](#).
- [7] F. Di Renzo and G. Erucci, “Thimble regularization at work: from toy models to chiral random matrix theories,” *Phys. Rev.* **D92** no. 8, (2015) 085030, [arXiv:1507.03858 \[hep-lat\]](#).
- [8] Y. Tanizaki, Y. Hidaka, and T. Hayata, “Lefschetz-thimble analysis of the sign problem in one-site fermion model,” *New J. Phys.* **18** no. 3, (2016) 033002, [arXiv:1509.07146 \[hep-th\]](#).
- [9] H. Fujii, S. Kamata, and Y. Kikukawa, “Monte Carlo study of Lefschetz thimble structure in one-dimensional Thirring model at finite density,” *JHEP* **12** (2015) 125, [arXiv:1509.09141 \[hep-lat\]](#). [Erratum: JHEP09,172(2016)].
- [10] A. Alexandru, G. Basar, and P. Bedaque, “Monte Carlo algorithm for simulating fermions on Lefschetz thimbles,” *Phys. Rev.* **D93** no. 1, (2016) 014504, [arXiv:1510.03258 \[hep-lat\]](#).
- [11] J. R. Klauder, “STOCHASTIC QUANTIZATION,” *Acta Phys. Austriaca Suppl.* **25** (1983) 251–281.
- [12] J. R. Klauder, “A Langevin Approach to Fermion and Quantum Spin Correlation Functions,” *J. Phys.* **A16** (1983) L317.
- [13] J. Berges and I. O. Stamatescu, “Simulating nonequilibrium quantum fields with stochastic quantization techniques,” *Phys. Rev. Lett.* **95** (2005) 202003, [arXiv:hep-lat/0508030 \[hep-lat\]](#).
- [14] J. Berges, S. Borsanyi, D. Sexty, and I. O. Stamatescu, “Lattice simulations of real-time quantum fields,” *Phys. Rev.* **D75** (2007) 045007, [arXiv:hep-lat/0609058 \[hep-lat\]](#).
- [15] J. Berges and D. Sexty, “Real-time gauge theory simulations from stochastic quantization with optimized updating,” *Nucl. Phys.* **B799** (2008) 306–329, [arXiv:0708.0779 \[hep-lat\]](#).
- [16] J. Bloch, J. Glesaaen, J. J. M. Verbaarschot, and S. Zafeiropoulos, “Complex Langevin Simulation of a Random Matrix Model at Nonzero Chemical Potential,” [arXiv:1712.07514 \[hep-lat\]](#).
- [17] G. Aarts and I.-O. Stamatescu, “Stochastic quantization at finite chemical potential,” *JHEP* **09** (2008) 018, [arXiv:0807.1597 \[hep-lat\]](#).
- [18] C. Pehlevan and G. Guralnik, “Complex Langevin Equations and Schwinger-Dyson Equations,” *Nucl. Phys.* **B811** (2009) 519–536, [arXiv:0710.3756 \[hep-th\]](#).

- [19] G. Aarts, “Can stochastic quantization evade the sign problem? The relativistic Bose gas at finite chemical potential,” *Phys. Rev. Lett.* **102** (2009) 131601, [arXiv:0810.2089 \[hep-lat\]](#).
- [20] G. Aarts, “Complex Langevin dynamics at finite chemical potential: Mean field analysis in the relativistic Bose gas,” *JHEP* **05** (2009) 052, [arXiv:0902.4686 \[hep-lat\]](#).
- [21] G. Aarts and K. Splittorff, “Degenerate distributions in complex Langevin dynamics: one-dimensional QCD at finite chemical potential,” *JHEP* **08** (2010) 017, [arXiv:1006.0332 \[hep-lat\]](#).
- [22] G. Aarts and F. A. James, “Complex Langevin dynamics in the SU(3) spin model at nonzero chemical potential revisited,” *JHEP* **01** (2012) 118, [arXiv:1112.4655 \[hep-lat\]](#).
- [23] Y. Ito and J. Nishimura, “The complex Langevin analysis of spontaneous symmetry breaking induced by complex fermion determinant,” *JHEP* **12** (2016) 009, [arXiv:1609.04501 \[hep-lat\]](#).
- [24] Y. Ito and J. Nishimura, “Spontaneous symmetry breaking induced by complex fermion determinant — yet another success of the complex Langevin method,” *PoS LATTICE2016* (2016) 065, [arXiv:1612.00598 \[hep-lat\]](#).
- [25] K. N. Anagnostopoulos, T. Azuma, Y. Ito, J. Nishimura, and S. K. Papadoudis, “Complex Langevin analysis of the spontaneous symmetry breaking in dimensionally reduced super Yang-Mills models,” *JHEP* **02** (2018) 151, [arXiv:1712.07562 \[hep-lat\]](#).
- [26] S. Hands, T. J. Hollowood, and J. C. Myers, “QCD with Chemical Potential in a Small Hyperspherical Box,” *JHEP* **07** (2010) 086, [arXiv:1003.5813 \[hep-th\]](#).
- [27] D. J. Gross and E. Witten, “Possible Third Order Phase Transition in the Large N Lattice Gauge Theory,” *Phys. Rev.* **D21** (1980) 446–453.
- [28] S. R. Wadia, “A Study of U(N) Lattice Gauge Theory in 2-dimensions,” [arXiv:1212.2906 \[hep-th\]](#).
- [29] S. R. Wadia, “ $N = \infty$ Phase Transition in a Class of Exactly Soluble Model Lattice Gauge Theories,” *Phys. Lett.* **93B** (1980) 403–410.
- [30] G. Parisi and Y.-s. Wu, “Perturbation Theory Without Gauge Fixing,” *Sci. Sin.* **24** (1981) 483.
- [31] P. H. Damgaard and H. Huffel, “Stochastic Quantization,” *Phys. Rept.* **152** (1987) 227.
- [32] G. Aarts, E. Seiler, and I.-O. Stamatescu, “The Complex Langevin method: When can it be trusted?,” *Phys. Rev.* **D81** (2010) 054508, [arXiv:0912.3360 \[hep-lat\]](#).
- [33] G. Aarts, F. A. James, E. Seiler, and I.-O. Stamatescu, “Complex Langevin: Etiology and Diagnostics of its Main Problem,” *Eur. Phys. J.* **C71** (2011) 1756, [arXiv:1101.3270 \[hep-lat\]](#).
- [34] G. Aarts, P. Giudice, and E. Seiler, “Localised distributions and criteria for correctness in complex Langevin dynamics,” *Annals Phys.* **337** (2013) 238–260, [arXiv:1306.3075 \[hep-lat\]](#).
- [35] P. V. Buividovich, G. V. Dunne, and S. N. Valgushev, “Complex Path Integrals and Saddles in Two-Dimensional Gauge Theory,” *Phys. Rev. Lett.* **116** no. 13, (2016) 132001, [arXiv:1512.09021 \[hep-th\]](#).
- [36] M. Marino, “Les Houches lectures on matrix models and topological strings,” 2004.

- [arXiv:hep-th/0410165](https://arxiv.org/abs/hep-th/0410165) [hep-th].
<http://weblib.cern.ch/abstract?CERN-PH-TH-2004-199>.
- [37] <https://dlmf.nist.gov/4.13>.
- [38] B. Sundborg, “The Hagedorn transition, deconfinement and N=4 SYM theory,” *Nucl. Phys.* **B573** (2000) 349–363, [arXiv:hep-th/9908001](https://arxiv.org/abs/hep-th/9908001) [hep-th].
- [39] O. Aharony, J. Marsano, S. Minwalla, K. Papadodimas, and M. Van Raamsdonk, “The Hagedorn - deconfinement phase transition in weakly coupled large N gauge theories,” *Adv. Theor. Math. Phys.* **8** (2004) 603–696, [arXiv:hep-th/0310285](https://arxiv.org/abs/hep-th/0310285) [hep-th]. [161(2003)].
- [40] L. Alvarez-Gaume, C. Gomez, H. Liu, and S. Wadia, “Finite temperature effective action, AdS(5) black holes, and 1/N expansion,” *Phys. Rev.* **D71** (2005) 124023, [arXiv:hep-th/0502227](https://arxiv.org/abs/hep-th/0502227) [hep-th].
- [41] L. Alvarez-Gaume, P. Basu, M. Marino, and S. R. Wadia, “Blackhole/String Transition for the Small Schwarzschild Blackhole of AdS(5) \times S⁵ and Critical Unitary Matrix Models,” *Eur. Phys. J.* **C48** (2006) 647–665, [arXiv:hep-th/0605041](https://arxiv.org/abs/hep-th/0605041) [hep-th].
- [42] T. D. Cohen, “Functional integrals for QCD at nonzero chemical potential and zero density,” *Phys. Rev. Lett.* **91** (2003) 222001, [arXiv:hep-ph/0307089](https://arxiv.org/abs/hep-ph/0307089) [hep-ph].
- [43] S. Hands, S. Kim, and J.-I. Skullerud, “A Quarkyonic Phase in Dense Two Color Matter?,” *Phys. Rev.* **D81** (2010) 091502, [arXiv:1001.1682](https://arxiv.org/abs/1001.1682) [hep-lat].
- [44] P. Basu and A. Mukherjee, “Dissolved deconfinement: Phase Structure of large N gauge theories with fundamental matter,” *Phys. Rev.* **D78** (2008) 045012, [arXiv:0803.1880](https://arxiv.org/abs/0803.1880) [hep-th].
- [45] D. Banerjee and S. Chandrasekharan, “Finite size effects in the presence of a chemical potential: A study in the classical non-linear O(2) sigma-model,” *Phys. Rev.* **D81** (2010) 125007, [arXiv:1001.3648](https://arxiv.org/abs/1001.3648) [hep-lat].
- [46] K. Nagata, J. Nishimura, and S. Shimasaki, “Argument for justification of the complex Langevin method and the condition for correct convergence,” *Phys. Rev.* **D94** no. 11, (2016) 114515, [arXiv:1606.07627](https://arxiv.org/abs/1606.07627) [hep-lat].
- [47] K. Nagata, J. Nishimura, and S. Shimasaki, “Testing the criterion for correct convergence in the complex Langevin method,” [arXiv:1802.01876](https://arxiv.org/abs/1802.01876) [hep-lat].